Journal of Organometallic Chemistry 879 (2019) 47–59

Contents lists available at ScienceDirect

Journal of Organometallic Chemistry

journal homepage: www.elsevier.com/locate/jorganchem

N-Acyclic carbene complexes supported by *meso*-$Ph_2PCH_2P(Ph)CH_2P(Ph)CH_2PPh_2$ (*meso*-dpmppm) as an asymmetric pincer ligand

Tomoaki Tanase*, Mari Urabe, Natsumi Mori, Satoko Hatada, Sayo Noda, Hiroe Takenaka, Kanako Nakamae, Takayuki Nakajima

Department of Chemistry, Faculty of Science, Nara Women's University, Kitauoya-nishi-machi, Nara, 630-8506, Japan

ARTICLE INFO

Article history:
Received 26 September 2018
Received in revised form
10 October 2018
Accepted 11 October 2018
Available online 13 October 2018

Dedicated to Professor Richard J. Puddephatt on the occasion of 75th birthday.

Keywords:
N-Acyclic carbene complex
Platinum
Iridium
PPP pincer
Tetraphosphine

ABSTRACT

Reaction of $[PtCl_2(cod)]$ with a tetraphosphine *meso*-bis[(diphenylphosphinomethyl)phenylphosphino] methane (*meso*-dpmppm), afforded mononuclear Pt^{II} complexes, $[PtCl(meso\text{-dpmppm}-\kappa^3)]X$ (X = Cl (**1a**), PF_6 (**1b**)); the *meso*-dpmppm ligand coordinates to the Pt^{II} ion tightly with two outer and one inner phosphorus atoms to form fused six- and four-membered chelate rings which is regarded as an asymmetric *PPP* pincer ligand bearing an uncoordinate inner phosphine unit. Complex **1** readily reacted with RNC in the presence of NH_4PF_6 to afford $[Pt(meso\text{-dpmppm}-\kappa^3)(RNC)](PF_6)_2$ (R = Xyl (**2a**), Cy (**2b**), ^{t}Bu (**2c**)). When **2a** and **2b** were reacted with excess of benzylamine ($BnNH_2$), *N*-acyclic carbene complexes, $[Pt(meso\text{-dpmppm}-\kappa^3)\{C(NHR)(NHBn)\}](PF_6)_2$ (R = Xyl (**3a**), Cy (**3c**)), were obtained, and a similar treatment of **2a** with *n*-octylamine ($C_8H_{17}NH_2$) afforded $[Pt(meso\text{-dpmppm}-\kappa^3)\{C(NHXyl)(NHC_8H_{17})\}](PF_6)_2$ (**3b**). In contrast, complex **2c** was transformed into a cyanide complex, $[Pt(CN)(meso\text{-dpmppm}-\kappa^3)]PF_6$ (**4**), through N–C(^{t}Bu) bond cleavage when heated at 80 °C with $BnNH_2$ or $PhNH_2$. Complexes **1**–**4** were characterized by ^{1}H and ^{31}P NMR and ESI-MS spectroscopies and X-ray diffraction analyses. The uncoordinate inner phosphine of **1b** is readily reacted with $[Cp^*MCl_2]_2$ to give heterodimetallic complexes, $[PtCl(\eta^5\text{-}Cp^*MCl_2)(\mu\text{-}meso\text{-dpmppm}-\kappa^3,\kappa^1)]PF_6$ (M = Ir (**5a**), Rh (**5b**); Cp^* = 1,2,3,4,5-pentamethylcyclopentadienyl). Complex **2a** also reacted with $[Cp^*IrCl_2]_2$ to yield $[Pt(\eta^5\text{-}Cp^*IrCl_2)(\mu\text{-}meso\text{-dpmppm}-\kappa^3,\kappa^1)(XylNC)]PF_6$ (**6a**) together with **5a**, and however, **6a** would not react with $BnNH_2$, just releasing XylNC to result in **5a**. Attachment of the metal fragment of $\{Cp^*IrCl_2\}$ to the uncoordinated phosphine caused a crucial conformational change of the six-membered chelate ring from a stable chair conformation to a twist-boat structure, which concomitantly reduced reactivity of the isocyanide ligand toward nucleophilic attack of the amine by steric hindrance of *meso*-dpmppm pincer ligand. These results could be recognized as on/off switching of the asymmetric $\{Pt^{II}(meso\text{-dpmppm}-\kappa^3)\}$ pincer complex.

1. Introduction

Synergistic effects of multinuclear metal centers are of growing interest in developing multimetallic catalytic systems, electronic, optical, and magnetic devices, and biomimetic functional molecules [1–7]. In this regard, design of multidentate ligands is crucial to construct the desired multinuclear systems. Recently, we have systematically synthesized a series of methylene-bridged linear tetraphosphine ligands, *meso* or *rac*-$Ph_2PCH_2P(Ph)(CH_2)_nP(Ph)CH_2PPh_2$ (n = 1 (dpmppm) [8–19], 2 (dpmppe) [20], 3 (dpmppp) [20–23]), to organize structurally constrained multinuclear metal centers, and in particular, demonstrated that *meso*/*rac*-dpmppm effectively stabilized versatile molecular metal chains, $[Pd_8(\mu\text{-}meso/rac\text{-dpmppm})_4L_2]^{4+}$ (L = none, acetonitrile, dmso, isocyanides) [17–19], $[Au_4(\mu\text{-}meso/rac\text{-dpmppm})_2]^{4+}$ [8,14], $[Ag_4(\mu\text{-}meso\text{-dpmppm})_2L_n]^{4+}$ (n = 2, 4; L = acetonitrile, isocyanides) [11], and $[Cu_4(\mu\text{-X})_3(\mu\text{-}meso\text{-dpmppm})_2L_2]^+$ and $[Cu_8(\mu\text{-X})_8(\mu\text{-}meso\text{-dpmppm})_2L_2]$ (X = Cl, Br, I; L = dmf. dmso, py, isocyanides) [10]. In addition, *meso*-dpmppm ligand has proven very flexible to support AuAgCu octanuclear rings, $\{[Au_2MCuCl_2(\mu\text{-}meso\text{-dpmppm})_2]_2\}^{4+}$ (M = Au, Ag, Cu) [11], and di and tetranuclear copper hydride complexes, $[Cu_2(\mu\text{-H})(\mu\text{-}meso\text{-dpmppm})_2]^+$ and $[Cu_4(\mu_4\text{-H})(\mu\text{-H})_2(\mu\text{-}meso\text{-dpmppm})_2]^+$ [15]. Furthermore, it nests a Pd^{II} mononuclear center in a pincer-type

* Corresponding author.
E-mail address: tanase@cc.nara-wu.ac.jp (T. Tanase).

https://doi.org/10.1016/j.jorganchem.2018.10.005
0022-328X/

fashion to form [PdCl(*meso*-dpmppm−κ^3)]$^+$ (**A**), in which six- and four-membered chelate rings are fused with an uncoordinated phosphine unit involved in the six-membered ring (Scheme 1) [12]. An addition of {Cp*MCl_2} fragment (M = Rh, Ir, Cp* = pentamethyl cyclopentadienyl) to the uncoordinated phosphine, forming dinuclear species of [PdCl(η^5−Cp*MCl_2)(μ−*meso*-dpmppm−κ^3,κ^1)]$^+$ (**B**), brought about conformational change of the six-membered ring from a stable chair to a twist-boat structure, which further destabilized the strained four-membered chelate ring and promoted a capture of the third metal ions via its ring-opening to construct heterotrimetallic complexes, [$PdCl_2$(η^5−Cp*M'Cl_2)(η^5−Cp*MCl_2)(μ−*meso*-dpmppm−κ^2,κ^1,κ^1)] (**C**) and [PdCl(μ−Cl)(η^5−Cp*M'Cl)(η^5−Cp*MCl_2)(μ−*meso*-dpmppm−κ^2,κ^1,κ^1)]PF_6 (**D**) (M, M' = Ir, Rh), in stepwise ways (Scheme 1).

In the present study, we have tried to prepare the Pt^{II} mononuclear complex, [PtCl(*meso*-dpmppm−κ^3)]$^+$ (**1**), analogous to **A** and found that the meridional *meso*-dpmppm tightly binds to Pt^{II} center as an asymmetric *PPP* pincer ligand, which is contrasted to the labile behavior of the Pd counterpart **A** as mentioned above. Since asymmetric pincer ligands are relatively difficult to synthesize in comparison with symmetric ones [24–28], and in addition, pincer ligands with all phosphorous donor sets have still been limited to few examples [29–31], we have been interested in the {Pt^{II}(*meso*-dpmppm−κ^3)} asymmetric pincer unit to explore new functional systems [28,32]. Complex **1** was converted by treating with isocyanide to [Pt(*meso*-dpmppm−κ^3)(RNC)]$^{2+}$ (R = 2,6-xylyl (Xyl, **2a**), cyclohexyl (Cy, **2b**), *tert*-butyl (^{t}Bu, **2c**)) and their reactions with amines were examined. Complexes **2a** and **2b** readily reacted with benzylamine ($BnNH_2$) at room temperature to afford *N*-acyclic diamino carbene complexes, [Pt(*meso*-dpmppm−κ^3){C(NHR)(NHBn)}]$^{2+}$ (**3**), and in contrast, **2c** was not reacted with $BnNH_2$ at r.t. and transformed into a cyanide complex, [Pt(CN)(*meso*-dpmppm−κ^3)]PF_6 (**4**) through N−C(^{t}Bu) bond cleavage when treated with $BnNH_2$ or $PhNH_2$ at 80 °C. The present results demonstrated that the reactivity of **2** depended on the substituent group of isocyanides, and the stereo-structures of the NAC pincer complexes also varied depending on the substituents of isocyanide and amine. Further, addition of {Cp*$IrCl_2$} to the uncoordinated phosphine of **2a** caused a conformational change of the six-membered chelate ring from a stable chair conformation to a twist-boat structure, which dramatically reduced its reactivity toward $BnNH_2$ by steric hindrance of *meso*-dpmppm pincer ligand. These phenomena could be considered as on/off switching of the asymmetric {Pt^{II}(*meso*-dpmppm−κ^3)} pincer complex. We wish to report herein synthesis, characterization, and reactivity of the pincer Pt^{II} complexes.

2. Results and discussion

2.1. Mononuclear Pt complexes with meso-dpmppm, [PtCl(meso-dpmppm−κ^3)]X (X = Cl (**1a**), PF_6 (**1b**) and [Pt(meso-dpmppm−κ^3)(RNC)]$(PF_6)_2$ (R = Xyl (**2a**), Cy (**2b**), ^{t}Bu (**2c**))

By treatment of [$PtCl_2$(cod)] with 1 equiv. of *meso*-dpmppm in dichloromethane, colorless crystals of [PtCl(*meso*-dpmppm−κ^3)]Cl (**1a**) were obtained in 51% yield. Complex **1a** was further converted with excess of NH_4PF_6 into [PtCl(*meso*-dpmppm−κ^3)]PF_6 (**1b**) in 76% yield (Scheme 2). Complexes **1a** and **1b** were characterized by elemental analysis, ^{1}H and ^{31}P{^{1}H} NMR and ESI−MS spectra, and X-ray crystallography to have an almost identical structure except the counter anion. Perspective views for the complex cations of **1a** and **1b** are shown in Fig. S1 (Supplementary Data (SD)) and the representative structural parameters are listed in Table S5 (SD). The structures of complex cations **1a** and **1b** involve a square planar Pt^{II} center coordinated by a *meso*-dpmppm ligand and a chloride anion. The *meso*-dpmppm ligand coordinates to the Pt atom with two outer (P1, P4) and one inner (P3) phosphorus atoms to form an asymmetric κ^3*PPP* pincer structure, where six- and four-membered chelate rings are fused, and the remaining inner P atom (P2) is uncoordinated. The six-membered ring takes a stable chair conformation and the phenyl group on P2 atom occupies an equatorial position. The P1−Pt1−P3 bite angles for six-membered

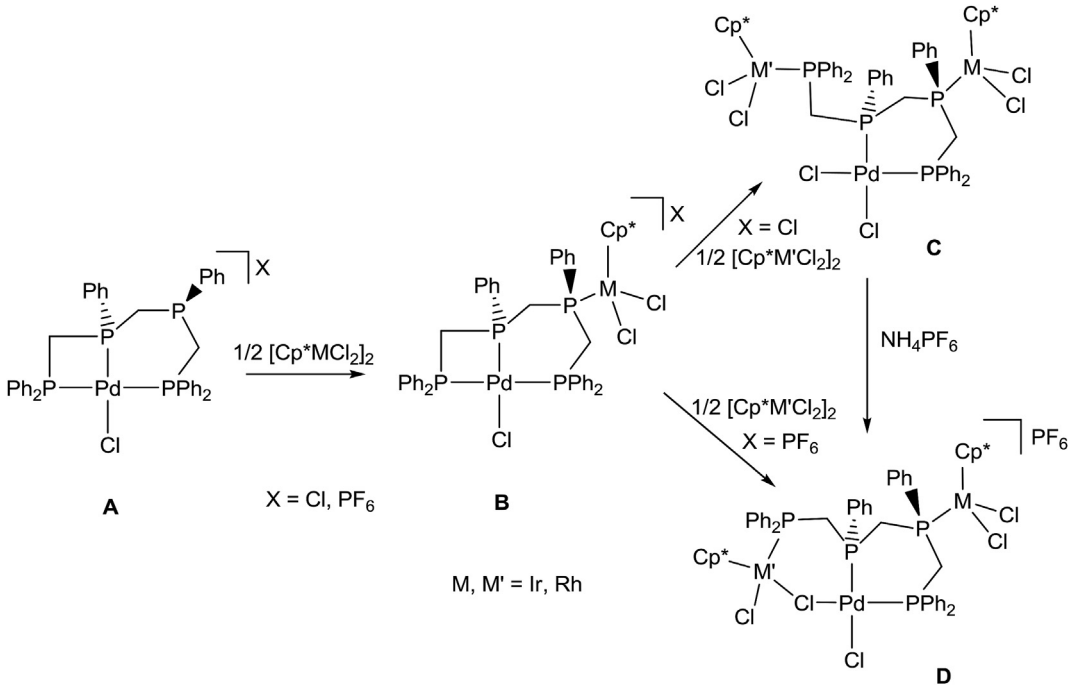

Scheme 1. Transformation of [PdCl(*meso*−dpmppm-κ^3)]X (**A**) to [PdCl(η^5−Cp*MCl_2)(μ−*meso*-dpmppm−κ^3,κ^1)]X (**B**), [$PdCl_2$(η^5−Cp*M'Cl_2)(η^5−Cp*MCl_2)(μ−*meso*-dpmppm−κ^2,κ^1,κ^1)] (**C**), and [PdCl(μ−Cl)(η^5−Cp*M'Cl)(η^5−Cp*MCl_2)(μ−*meso*-dpmppm−κ^2,κ^1,κ^1)]PF_6 (**D**) (X = Cl, PF_6; M, M' = Ir, Rh).

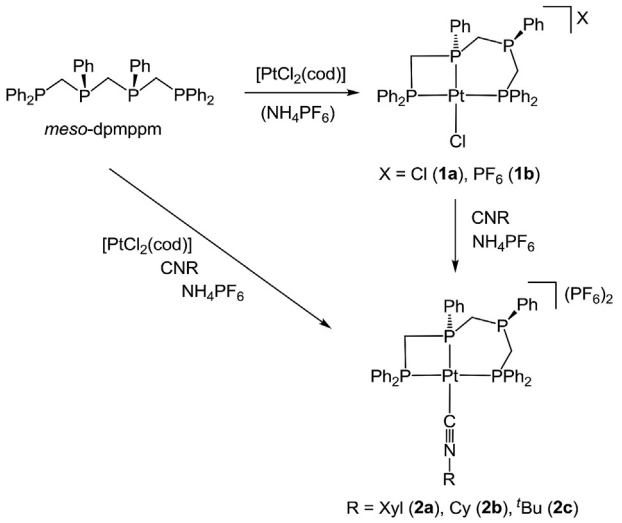

Scheme 2. Preparations of [PtCl(*meso*-dpmppm−κ^3)]X (X = Cl (**1a**), PF_6 (**1b**)) and [Pt(*meso*-dpmppm−κ^3)(RNC)]$(PF_6)_2$ (R = Xyl (**2a**), Cy (**2b**), ^{t}Bu (**2c**)).

ring are 96.83(3)° (**1a**) and 98.90(2)° (**1b**), and the P3−Pt1−P4 angles for four-membered ring are 71.86(2)° (**1a**) and 71.88(2)° (**1b**). The bicyclic chelate ring system constrains three phenyl groups of P1, P3, and P4 atoms to axial direction (**ax**) with respect to the Pt square plane (Closed side in Fig. S2 (right)), and the other three phenyl groups are in equatorial orientation (**eq**) on the other side of the plane (Open side in Fig. S2 (left)), onto which the counter anion Cl^- or PF_6^- is loosely incorporated. These structural features are closely similar to those of the Pd^{II} counterparts, [PdCl(*meso*-dpmppm-κ^3)]X (X = Cl, PF_6) [12].

The asymmetric *PPP* pincer structure of {Pt(*meso*-dpmppm−κ^3)} of **1a**,**b** confirmed by the X-ray analyses is very stable in the solution states, which was evident in ^{1}H and ^{31}P NMR spectra (see Figs. S7a,b and Table 1). The ^{31}P{^{1}H} NMR spectrum of **1a** in $CDCl_3$ showed four resonances with ^{195}Pt satellite peaks at δ −36.7 ($^1J_{PtPA}$ = 1992 Hz), −47.7 ($^1J_{PtPB}$ = 2831 Hz), −39.6, and 3.9 ($^1J_{PtPD}$ = 2503 Hz) (Table 1), which are assignable to P_A, P_B, P_C, and P_D atoms in the light of PP′ coupling constants ($J_{PP'}$) and 2D NMR (^{1}H−^{1}H and ^{31}P−^{31}P COSY and ^{1}H−^{31}P HMBC) techniques (the labels of phosphorus atoms are indicated in Table 1). The large *trans* PP' coupling ($^2J_{PAPD}$) of 419 Hz clearly demonstrated the asymmetric κ^3*PPP* pincer structure retained in the solution. The ESI−MS spectra of **1a** and **1b** showed the complex cation peak of [PtCl(dpmppm)]$^+$ at *m*/*z* = 859.185 and 859.202 (*z* = 1), respectively (Figs. S11a,b).

When [$PtCl_2$(cod)] was reacted with 1 equiv. of *meso*-dpmppm and isocyanide (RNC) in the presence of excess NH_4PF_6, a series of isocyanide complexes, [Pt(*meso*-dpmppm−κ^3)(RNC)]$(PF_6)_2$ (R = Xyl (**2a**), Cy (**2b**), ^{t}Bu (**2c**)), were obtained in moderate yields (47−68%). Complexes **2a**−**c** were also prepared from **1b** by treatment with RNC and NH_4PF_6. The structures of **2a**−**c** were determined by X-ray diffraction analyses to possess an almost identical structure (Figs. S3a,b), where the chloride anion of **1** was replaced by a terminal isocyanide and the *meso*-dpmppm ligand tightly binds to Pt^{II} center in asymmetric κ^3*PPP* meridional mode (Pt1−C1 = 2.011(13) Å (**2a**), 1.996(3) Å (**2b**), 2.010(4) Å (**2c**); C1−N1 = 1.130(18) Å (**2a**), 1.136(5) Å (**2b**), 1.131(6) Å (**2c**)). The {Pt(*meso*-dpmppm−κ^3)} pincer structure is not altered from **1a**,**b** (Table S6), in which the three axial phenyl groups protected Closed side of Pt^{II} coordination plane, and the equatorial phenyl groups surrounded Open side (Fig. S4). The IR spectra showed a peak of C≡N stretching vibration at 2200 cm^{-1} (**2a**), 2238 cm^{-1} (**2b**), and 2234 cm^{-1} (**2c**), which are usual values for terminal isocyanide ligated to Pt^{II} center [33]. The ^{31}P{^{1}H} NMR spectra of **2a**−**c** also exhibited identical spectral patterns, while $^2J_{PAPD}$ of 316−322 Hz significantly decreased from that of **1b** (419 Hz), and the $^1J_{PtP}$ coupling constants are all appreciably smaller than those of **1b** (Table 1). For example, in the ^{31}P{^{1}H} NMR spectrum of **2a**, four resonances appeared at δ_{PA} −36.2 ($^1J_{PtPA}$ = 1774 Hz), δ_{PB} −50.0 ($^1J_{PtPB}$ = 2308 Hz), δ_{PC} −42.0, and δ_{PD} −1.0 ($^1J_{PtPD}$ = 2248 Hz) with $^2J_{PAPD}$ = 322 Hz. These propensities may be attributable to larger *trans* influence and steric bulkiness of the isocyanide ligand than those of chloride.

2.2. *N*-Acyclic carbene Pt complexes with meso-dpmppm, [Pt(meso-dpmppm−κ^3){C(NHR)(NHR′)}](PF$_6$)$_2$ (R = Xyl, R′ = Bn (**3a**), C_8H_{17} (**3b**); R = Cy, R′ = Bn (**3c**)), and [Pt(CN)(meso-dpmppm−κ^3)]PF$_6$ (**4**)

Since Pd^{II} and Pt^{II} complexes of *N*-acyclic diamino carbene ligands have been well known to be derived from their parent isocyanide complexes [30], complexes **2a**−**c** were treated with various amines to examine their reactivity. Reaction of **2a** with an excess amount of benzylamine ($BnNH_2$) at room temperature afforded a *N*-acyclic carbene Pt^{II} complex formulated as [Pt(*meso*-dpmppm−κ^3){C(NHXyl)(NHBn)}]$(PF_6)_2$ (**3a**) in 54% yield (Scheme 3). A similar reaction with *n*-octylamine ($C_8H_{17}NH_2$) also gave birth to [Pt(*meso*-dpmppm−κ^3){C(NHXyl)(NHC$_8$H$_{17}$)}]$(PF_6)_2$ (**3b**) in 49% yield. Notably, aromatic amines such as aniline ($PhNH_2$), 4-toluidine (*p*-TolNH_2), and 2,6-xylidine (XylNH_2) no longer reacted with **2a** at all. In the IR spectra of **3a**,**b**, the C≡N stretching band found in **2a** disappeared and instead, N−H and C=N stretching bands were observed at 3386−3314 cm^{-1} and 1561−1546 cm^{-1}, respectively. The ESI−MS spectra of **3a** and **3b** in acetone showed the complex cation peaks of [Pt(*meso*-dpmppm−κ^3){C(NHXyl)(NHR′)}]$^{2+}$ at *m*/*z* = 530.648 (*z* = 2) (**3a**) and 541.684 (*z* = 2) (**3b**), and {[Pt(*meso*-dpmppm−κ^3){C(NHXyl)(NHR′)}]PF_6}$^+$ at *m*/*z* = 1206.305 (*z* = 1) (**3a**) and 1228.471 (*z* = 1) (**3b**) (Figs. S13a,b).

The structures of **3a**,**b** were determined by X-ray crystallography to reveal that the terminal XylNC ligand was converted to a *N*-acyclic diamino carbene ligand (NAC) of {C(NHXyl)(NHR′)} (R′ = Bn, C_8H_{17}) on the {Pt^{II}(*meso*-dpmppm−κ^3)} asymmetric pincer scaffold (Figs. 1 and 2, Fig. S5, and Table S7). In the structure of **3a** (Fig. 1), the NAC of {C(NHXyl)(NHBn)} coordinates to the Pt center with Pt1−C1 = 2.091(6) Å, Pt1−P3 = 2.310(2) Å, and P3−Pt1−C1 = 170.2(2)°. The Pt^{II}−C_{NAC} bond length fall within the normal range [34−38], and the Pt1−P3 distance appreciably increased from **2a** (2.287(3) Å) due to stronger *trans* influence of the NAC ligand than XylNC. The C1−N1 and C1−N2 bond distances of 1.314(8) Å and 1.325(8) Å are suggestive of large contribution of C=N double bond character into the resonance structure of NAC ligand, and the N1−C1−N2 angle of 118.9(6)° also indicates sp^2 character of the carbene C atom. The dihedral angle between the Pt coordination plane [Pt1P1P3P4C1] and the NAC plane [C1N1N2] is 83.1°, nearly perpendicular arrangements as usually observed in Pt^{II} and Pd^{II} complexes with NHC and NAC ligands [34−41].

In the perpendicular conformation, two stereoisomers with respect to the asymmetric {Pt(*meso*-dpmppm−κ^3)} plane are postulated as rotamers **A** and **B** (Scheme 4), and however, the present reaction afforded only one isomer of rotamer **B**, which did not exhibit any dynamic behaviors for the rotation around Pt−C_{NAC} bond and resulted from higher stability of rotamer **B** than **A** as estimated with steric factors (vide infra). In the structure of **3a**, the Xyl group is constrained to Closed side and the Bn group is directed to Open side (Fig. 1b). Furthermore, it is well known that NAC ligand adopts two different diastereomeric structures, denoted as *syn* and *anti*, with respect to Pt−C−N−R geometrical arrangement (Scheme 5), and the NAC ligand in **3a** takes *anti*-Xyl/*syn*-Bn

Table 1
$^{31}P\{^{1}H\}$ NMR spectral data of **1a,b**, **2a-c**, **3a-c**, **4**, **5a,b**, and **6a** showing chemical shifts δ, and $^{1}J_{PtP}$ and $J_{PP'}$ coupling constants (Hz).[a]

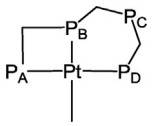

Comp.	δP$_A$ ($^{1}J_{PtPA}$)	δP$_B$ ($^{1}J_{PtPB}$)	δPc ($^{1}J_{PtPC}$)	δP$_D$ ($^{1}J_{PtPD}$)	J_{PAPB}	J_{PAPD}	J_{PBPC}	J_{PBPD}	J_{PCPD}
1a[b]	−36.7 (1992)	−47.7 (2831)	−39.6	3.9 (2503)	68	419	69	15	46
1b[c]	−40.2 (1956)	−51.5 (2721)	−40.0	6.0 (2466)	67	419	70	14	45
2a	−36.2 (1774)	−50.0 (2308)	−42.0	−1.0 (2248)	69	322	73	19	36
2b	−36.0 (1774)	−50.6 (2296)	−41.7	−1.5 (2260)	63	316	109	18	61
2c	−36.2 (1749)	−50.4 (2272)	−41.7	−1.7 (2260)	69	322	85	18	49
3a	−36.2 (2017)	−47.3 (1664)	−46.9	−2.2 (2515)	55	340	85	19	61
3b	−35.9 (2138)	−47.1 (1689)	−46.0	−1.0 (2527)	60	340	85	19	61
3c	major: minor = 1.2: 1								
(major)	−29.3 (2017)	−48.6 (1582)	−42.8	3.2 (2478)	59	337	85	23	66
(minor)	−30.2 (2017)	−48.8 (1582)	−43.8	2.3 (2478)	59	337	83	23	66
4	−37.8 (1907)	−54.0 (2005)	−39.4	0.3 (2369)	62	352	85	19	49
5a	−52.6 (1907)	−60.4 (2770)	−1.9	−9.5 (2381)	62	401	26	11	21
5b	−52.5 (1944)	−60.0 (2770)	30.2 (149)[d]	−8.7 (2381)	61	413	32	10	27
6a	−51.5 (1749)	−64.8 (2260)	−0.5	−4.7 (2174)	61	308	29	16	26

[a] Measured in CD_2Cl_2 at room temperature (except **1a** and **1b**).
[b] Measured in $CDCl_3$.
[c] Measured in acetone-d_6.
[d] $^{1}J_{RhP}$ (Hz).

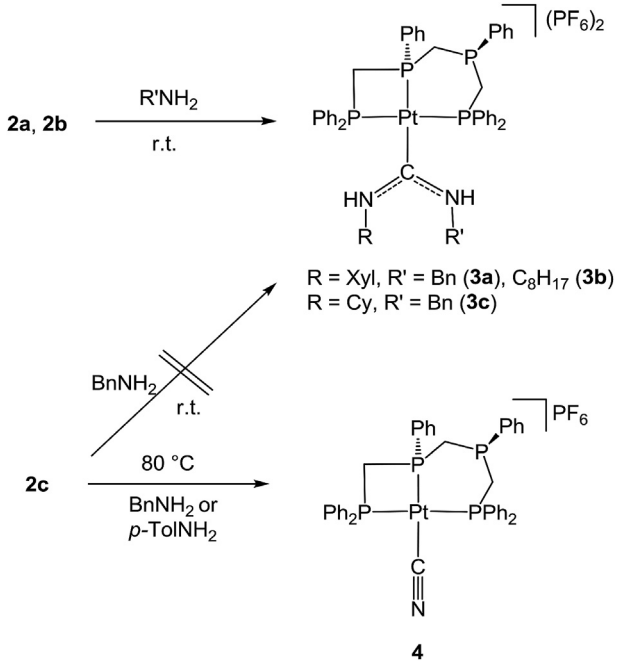

Scheme 3. Preparations of [Pt(*meso*-dpmppm−κ^3){C(NHR)(NHR′)}](PF$_6$)$_2$ (R = Xyl, R′ = Bn (**3a**), C_8H_{17} (**3b**); R = Cy, R′ = Bn (**3c**)), and [Pt(CN)(*meso*-dpmppm−κ^3)]PF$_6$ (**4**).

structure, tentatively ascribable to steric interactions between Xyl, Bn, and phenyl groups of *meso*-dpmppm. Based on the space-filling diagrams in Fig. 1b, the Xyl group should be directed to *anti*-position from repulsive interaction with axial phenyl groups, and the Bn group might be directed to *syn*-orientation owing to π−π stacking interaction with the equatorial phenyl group on P4 atom (dist. ~3.4 Å). It should be noted that **3a** did not undergo any interconversion between the *syn* and *anti*-isomers on the basis of VT NMR study up to 50 °C.

In the structure of **3b** (Fig. 2a), the NAC ligand {C(NHXyl)(NHC$_8$H$_{17}$)} attaches to the {Pt(*meso*-dpmppm−κ^3)}$^{2+}$ pincer unit with Pt1−C1 = 2.073(6) Å, Pt1−P3 = 2.306(2) Å, and P3−Pt1−C1 = 168.4(2)°. The C1−N1 and C1−N2 bond distances are 1.336(7) Å and 1.330(9) Å, and the N1−C1−N2 angle is 121.7(6)°, which are mostly same as those found in **3a**. The NAC plane [C1N1N2] is nearly perpendicular to the Pt^{II} coordination plane [PtP1P3P4C1] with a dihedral angel of 80.4°, where the Xyl group is located in *anti*-position of Closed side, and *n*-octyl group is oriented in *anti*-position of Open side (Fig. 2b), both resulting from avoiding repulsive interactions between the substituents of NAC and phenyl groups of *meso*-dpmppm.

When **2b** with CyNC was treated with BnNH$_2$ under the same conditions for **3a**, an analogous NAC complex, [Pt(*meso*-dpmppm−κ^3){C(NHCy)(NHBn)}](PF$_6$)$_2$ (**3c**) was obtained in 45% yield. The IR spectrum showed N−H and C≡N stretching bands at 3395/3341 cm^{-1} and 1570 cm^{-1}, respectively, and the ESI−MS

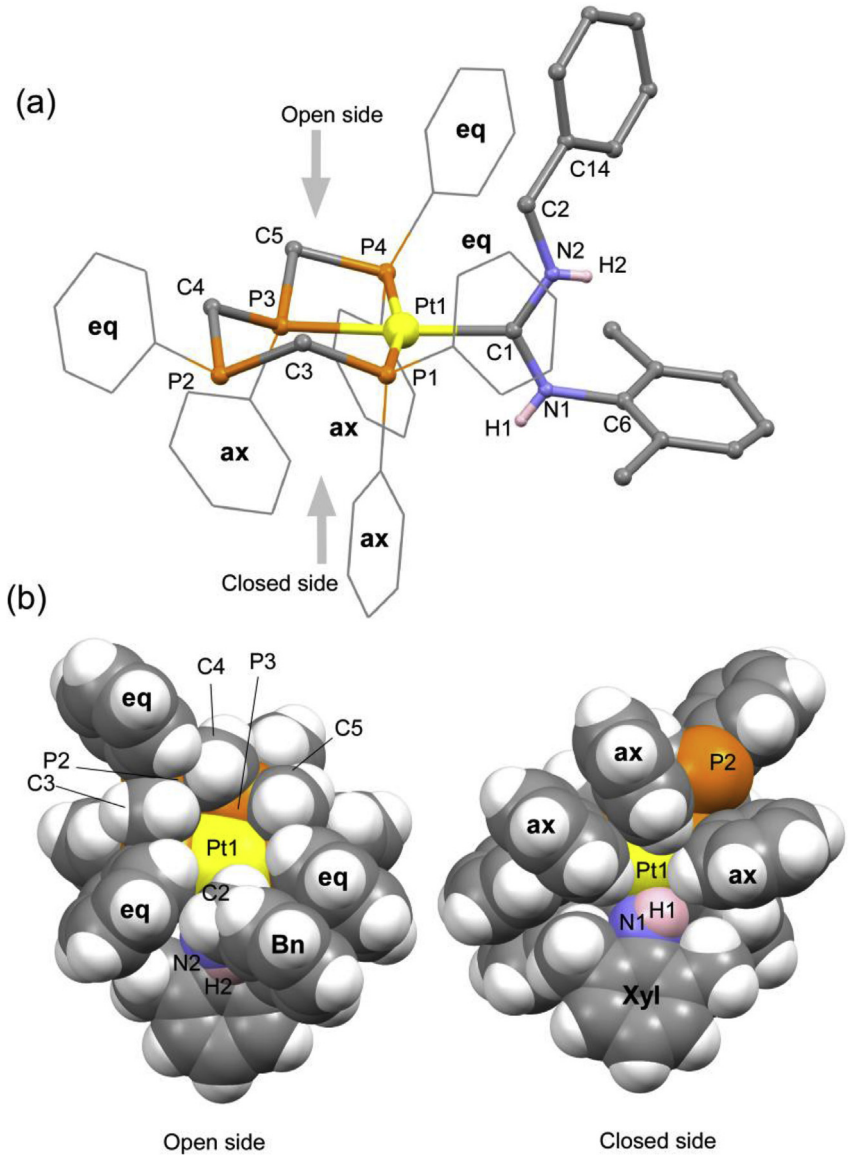

Fig. 1. (a) Perspective view for the complex cation of [Pt(*meso*-dpmppm−κ^3){C(NHXyl)(NHBn)}](PF$_6$)$_2$ (**3a**), and (b) space-filling views for the complex cation of **3a** from Open side (left) and Closed side (right). **eq** indicates equatorially oriented phenyl groups of *meso*-dpmppm and **ax** indicates axially oriented ones.

spectrum exhibited the cation peak of {[Pt(*meso*-dpmppm−κ^3){C(NHCy)(NHBn)}]PF$_6$}$^+$ at *m/z* = 1184.290 (*z* = 1) (Fig. S13c). The crystal structure of the complex cation of **3c** is illustrated in Fig. 3 and S5, and the selected structural parameters are listed in Table S7. The NAC ligand {C(NHCy)(NHBn)} is bound to the {Pt(*meso*-dpmppm−κ^3)}$^{2+}$ unit with Pt1−C1 = 2.079(10) Å, Pt1−P3 = 2.305(2) Å, P3−Pt1−C1 = 163.8(2)°, C1−N1 = 1.285(13) Å, C1−N2 = 1.341(12) Å, N1−C1−N2 = 119.3(9)°. The dihedral angle of [C1N1N2] vs. [PtP1P3P4C1] is 87.6°. While these structural features are essentially similar to those observed in **3a** and **3b**, the *syn*/*anti* conformation of {C(NHCy)(NHBn)} is different from those of **3a**,**b**; the Cy group is in *syn*-position of Closed side, and the Bn group is oriented in *anti*-position of Open side (Fig. 3b).

In comparison with the *anti*-Xyl/*syn*-Bn arrangement of **3a**, the observed *syn*-Cy/*anti*-Bn dispositions of **3c** is entirely different although the reasons are not clear, and may imply a probability of *anti*-Cy/*syn*-Bn isomer existing in the solution, which may be evident in the ^{31}P{^{1}H} NMR spectrum of **3c** (vide infra). In the NAC complexes **3a**−**c**, the isocyanide substituent is always directed in Closed side of the {Pt(*meso*-dpmppm−κ^3)}$^{2+}$ pincer plane, and in turn, the amine substituent is oriented in Open side, which implied that a nucleophilic attack of amine onto the isocyanide C≡N carbon occurred from Open side so as to avoid steric repulsive interactions with phenyl groups of the pincer ligand.

In the ^{31}P{^{1}H} NMR spectrum of **3a** in CD_2Cl_2, four resonances were observed at δ_{PA} −36.2 ($^1J_{PtPA}$ = 2017 Hz), δ_{PB} −47.3 ($^1J_{PtPB}$ = 1664 Hz), δ_{PC} −46.9, and δ_{PD} −2.2 ($^1J_{PtPD}$ = 2515 Hz) (Table 1, Fig. S9a). The *trans* PP' coupling ($^2J_{PAPD}$) of 340 Hz is close to **2a** (322 Hz). These spectral features are essentially similar to those of **2a**, demonstrating that the {Pt(*meso*-dpmppm−κ^3)}$^{2+}$ pincer units is firmly retained in the solution state, although the ^{195}Pt−P$_B$ coupling constant (1664 Hz) is considerably reduced from 2248 Hz in **2a**, due to stronger σ−donating ability of the NAC ligand. While the ^{31}P{^{1}H} NMR spectrum of **3b** showed the spectral patterns similar to those of **3a** (Table 1, Fig. S9b), that of **3c** demonstrated the presence of two isomers with two sets of four characteristic peaks as major species at δ −29.3 ($^1J_{PtPA}$ = 2017 Hz), −48.6 ($^1J_{PtPB}$ = 1582 Hz), −42.8, and 3.2 ($^1J_{PtPD}$ = 2478 Hz) and as minor

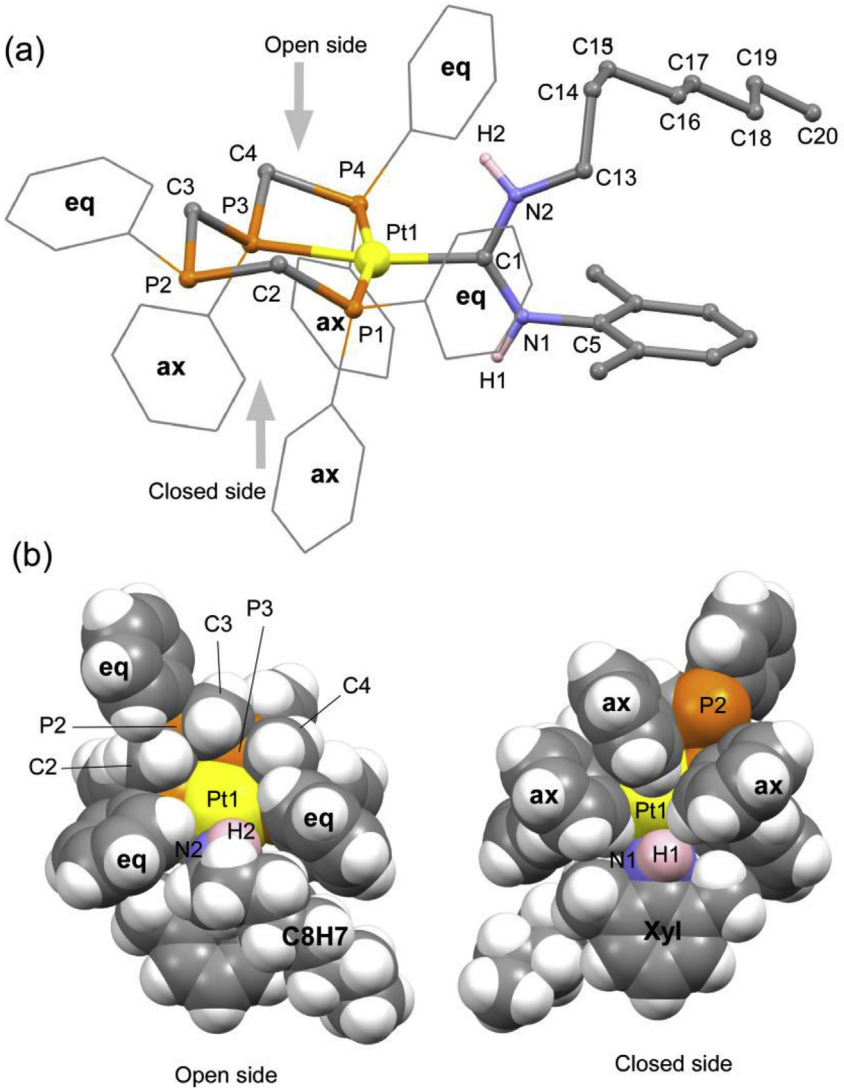

Fig. 2. (a) Perspective view for the complex cation of [Pt(*meso*-dpmppm−κ^3){C(NHXyl)(NHC$_8$H$_{17}$)}](PF$_6$)$_2$ (**3b**), and (b) space-filling views for the complex cation of **3b** from Open side (left) and Closed side (right). **eq** indicates equatorially oriented phenyl groups of *meso*-dpmppm and **ax** indicates axially oriented ones.

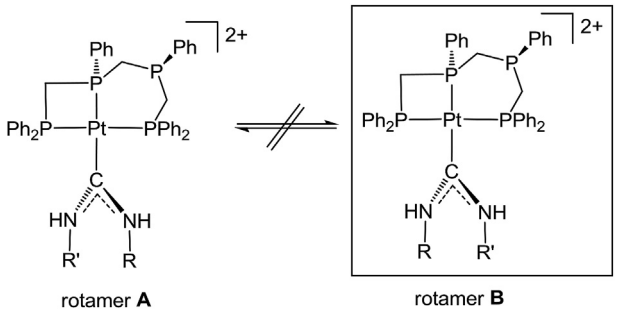

Scheme 4. Stereoisomers, rotamers **A** and **B**, for [Pt(*meso*-dpmppm−κ^3){C(NHR)(NHR′)}]$^{2+}$ (R is isocyanide substituent, R′ is amine substituent).

species at δ −30.2 ($^1J_{PtPA}$ = 2017 Hz), −48.8 ($^1J_{PtPB}$ = 1582 Hz), −43.8, and 2.3 ($^1J_{PtPD}$ = 2478 Hz) for P_A, P_B, P_C, and P_D atoms, respectively (Fig. S9c). The major and minor ratio is ca. 1.2: 1, and the chemical shifts and $^1J_{PtP}$ coupling constants are very close to each other, suggesting that these isomers are proposed to have *syn*-Cy/*anti*-Bn and *anti*-Cy/*syn*-Bn structures on the basis of steric consideration with the crystal structure of **3c** as mentioned above. The spectral patterns and their intensity ratios were not altered in variable temperature $^{31}P\{^1H\}$ NMR spectra from r.t to 50 °C.

When **2c** with ^{t}BuNC was treated with excess BnNH$_2$ at room temperature, the corresponding NAC complex was not formed at all and the isocyanide complex **2c** was recovered quantitatively. Whereas **2c** was inert for other amines at room temperature, assumingly due to steric bulkiness of ^{t}BuNC, when heated at 80 °C with BnNH$_2$ or *p*-TolNH$_2$, **2c** was readily converted to a cyanide complex, [Pt(CN)(*meso*-dpmppm−κ^3)]PF$_6$ (**4**) through N–C(^{t}Bu) bond cleavage in 67% isolated yield. The IR spectrum showed a C≡N stretching band at 2147 cm^{-1}, and in the ESI-MS spectrum, the complex cation peak of [Pt(CN)(*meso*-dpmppm)]$^+$ was observed at *m/z* 849.204 (*z* = 1) (Fig. S11c). The $^{31}P\{^1H\}$ NMR spectrum showed four resonances at δ −37.8 ($^1J_{PtPA}$ = 1907 Hz), −54.0 ($^1J_{PtPB}$ = 2005 Hz), −39.4, and 0.3 ($^1J_{PtPD}$ = 2369 Hz) with $^2J_{PAPD}$ = 352 Hz (Table 1 and Fig. S7c). The structure of **4** was determined by X-ray crystallography (Fig. S1c in SD) to possess a similar structure to **1b**, in which Cl$^-$ was replaced by CN$^-$ with Pt1–C1 = 2.080(7) Å, C1–N1 = 1.053(10) Å, P3–Pt1–C1 = 170.4(2)°, and Pt1–C1–N1 = 175.3(7)° (Table S5). Because the ^{31}P NMR

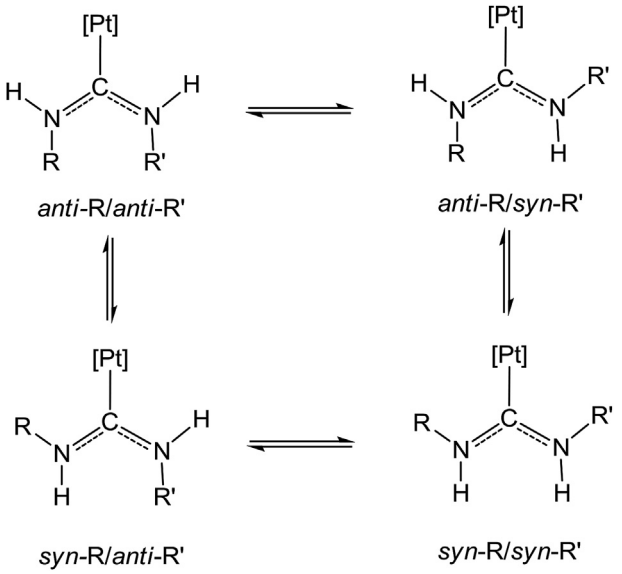

Scheme 5. Possible *syn* and *anti*-arrangements of R (isocyanide substituent) and R' (amine substituent) groups. [Pt] = {Pt(*meso*-dpmpppm−κ^3)}$^{2+}$.

spectra of the reaction mixture did not exhibit any intermediate species including the corresponding NAC complex, the N–C(^{t}Bu) bond cleavage mechanism may involve a dissociation of ^{t}Bu$^+$ carbocation promoted by amine as base, tentatively leading to its ammonium and halide adducts as well as isobutene which were monitored by ^{1}H NMR spectrum. The similar N–C(^{t}Bu) bond cleavage reaction of ^{t}BuNC was reported in {Ni^{II}(PNP)} and {Au^{III}(CNC)} pincer complexes [42,43] and in {(η^5–C_5H_4Me)Fe}$_4$ cluster chemistry [44].

2.3. PtM heterobimetallic complexes of [PtCl(η^5–Cp*MCl$_2$)(μ–dpmpppm–κ^3,κ^1)]PF$_6$ (M = Ir (**5a**), Rh (**5b**))

In order to incorporate a {Cp*MCl$_2$} fragment (M = Ir, Rh) onto the uncoordinated phosphine unite of the asymmetric pincer complex {Pt^{II}(*meso*-dpmpppm–κ^3)}, **1b** was reacted with 0.5 equiv of [Cp*MCl$_2$]$_2$ to afford [PtCl(η^5–Cp*MCl$_2$)(μ–*meso*-dpmpppm–κ^3,κ^1)]PF$_6$ (M = Ir (**5a**), Rh (**5b**)) in 66 and 36% yields, respectively (Scheme 6). Complexes **5a**,**b** were quite stable in the solution state, and did not react with another 0.5 equiv. of [Cp*MCl$_2$]$_2$, which interestingly contrasted to the labile Pd^{II} analogue [PdCl(η^5–Cp*MCl$_2$)(μ–*meso*-dpmpppm–κ^3,κ^1)]$^+$ (**B**), leading to the PdMM′ heterotrimetallic complexes,

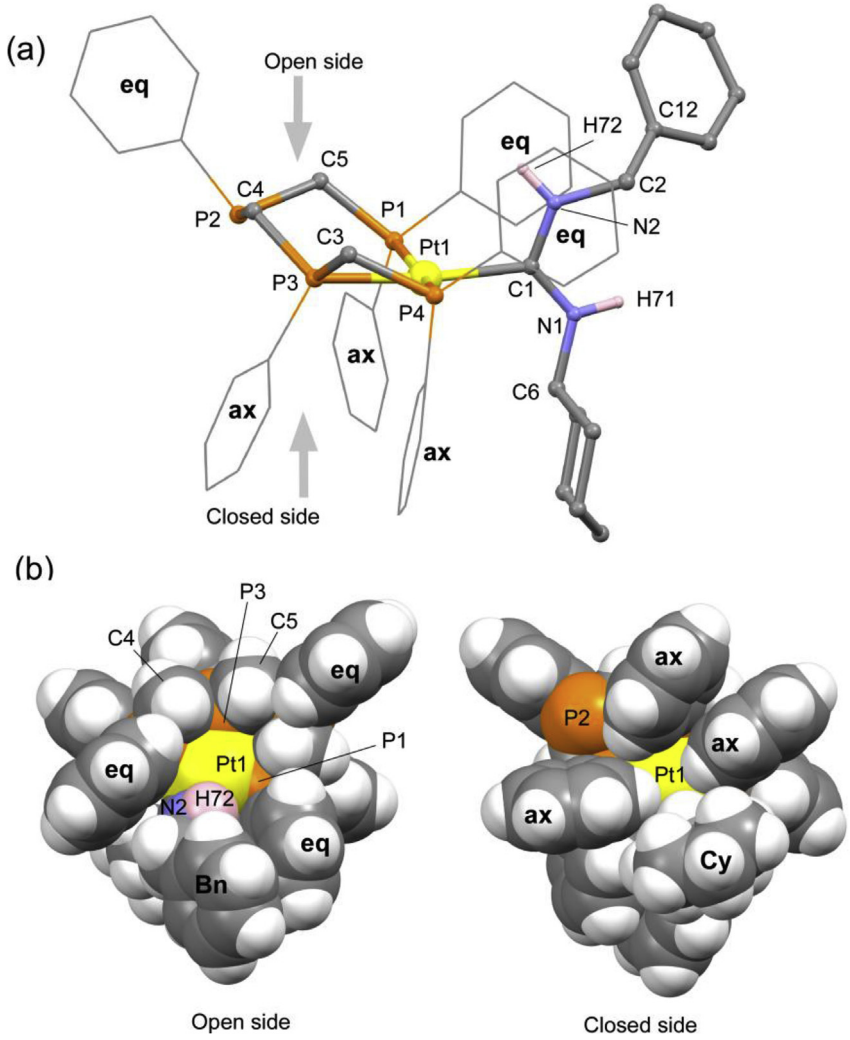

Fig. 3. (a) Perspective view for the complex cation of [Pt(*meso*-dpmpppm–κ^3){C(NHCy)(NHBn)}](PF$_6$)$_2$ (**3c**), and (b) space-filling views for the complex cation of **3c** from Open side (left) and Closed side (right). **eq** indicates equatorially oriented phenyl groups of *meso*-dpmpppm and **ax** indicates axially oriented ones.

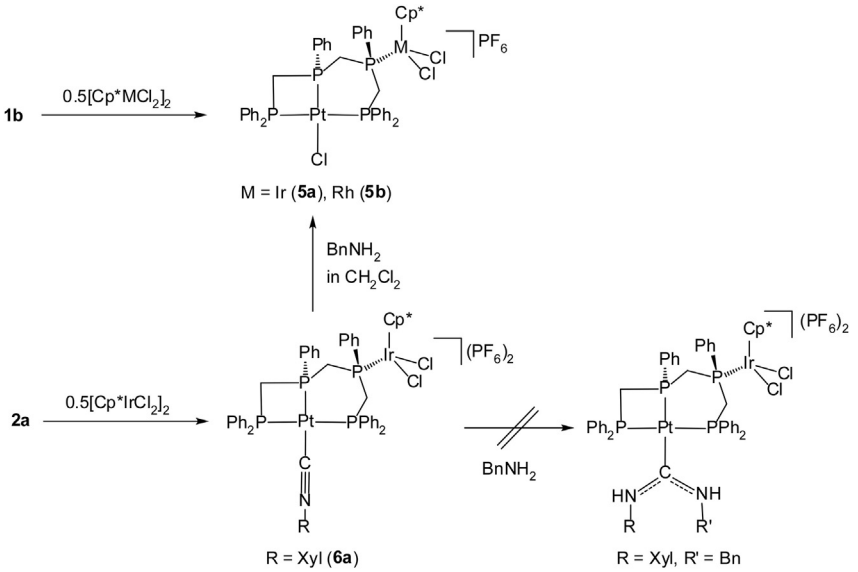

Scheme 6. Preparations of $[PtCl(\eta^5\text{–}Cp^*MCl_2)(\mu\text{–}meso\text{-dpmppm}\text{–}\kappa^3,\kappa^1)]PF_6$ (M = Ir (**5a**), Rh (**5b**)), and reaction of **2a** with $[Cp^*IrCl_2]_2$, and then, $BnNH_2$ to give **5a**.

$[PdCl_2(\eta^5\text{–}Cp^*M'Cl_2)(\eta^5\text{–}Cp^*MCl_2)(\mu\text{–}meso\text{-dpmppm}\text{–}\kappa^2,\kappa^1,\kappa^1)]$ and $[PdCl(\mu\text{–}Cl)(\eta^5\text{–}Cp^*M'Cl)(\eta^5\text{–}Cp^*MCl_2)(\mu\text{–}meso\text{-dpmppm}\text{–}\kappa^2,\kappa^1,\kappa^1)]^+$ (M, M' = Ir, Rh) (Scheme 1) [12], and hence, revealed that the asymmetric $\{Pt^{II}(meso\text{-dpmppm}\text{–}\kappa^3)\}$ pincer unit is considerably robust compared to the Pd^{II} counterpart.

In the $^{31}P\{^1H\}$ NMR spectra (Fig. S10 and Table 1), large *trans* PP' couplings were observed for the peaks of P_A and P_D ($^2J_{PAPD} = 401$ (**5a**), 413 (**5b**) Hz), which are comparable to the value of **1b** (420 Hz). The peaks for P_A, P_B, and P_D shifted to lower frequency side from those of **1b**, and the peaks for P_C were significantly higher energy shifted at δ −1.8 (**5a**) and 30.3 (**5b**); the latter was observed as a doublet of multiplets with $^1J_{RhP} = 149$ Hz. The ESI–MS spectra of **5a**,**b** in acetone showed the parent peaks at *m/z* = 1257.235 and 1167.128, which were assigned to $[PtCl(Cp^*MCl_2)(dpmppm)]^+$ (*m/z* = 1257.127 (M = Ir), 1167.070 (M = Rh)) (Fig. S14).

The structures of **5a** and **5b** were determined by X-ray crystallography (Fig. S6) to be isomorphous to each other; a perspective view for the complex cation of **5a** is given in Fig. 4 and the structural parameters are listed in Table S6. The complex cation of **5a** contains a square planar Pt^{II} center with *meso*-dpmppm–κ^3 asymmetric pincer ligand, which further bind to a $\{Cp^*MCl_2\}$ fragment through the uncoordinated inner phosphine unit (P2). The [PtPCPCP] six-membered ring adopts a twist-boat conformation as observed in the Pd^{II} analogue **B** (Scheme 1) [12]. In relation to the conformational change, the $\{Cp^*IrCl_2\}$ and Ph groups bound to P2 atom occupy the equatorial and axial sites, respectively, and the Pt1···P2 distance (3.881 Å (**5a**), 3.880 Å (**5b**)) is appreciably reduced from that of **1b** (3.986 Å). As a result of the conformational change induced by the addition of $\{Cp^*IrCl_2\}$ on P2 atom, Open side of the Pt^{II} coordination plane (in **1b**) is sterically protected by the axial phenyl group on P2 atom in **5a** (Fig. 4b (left) and Fig. S2b (left)).

In order to elucidate effects of the conformational change on reactivity of the isocyanide ligand bound to the $\{Pt^{II}(meso\text{-dpmppm})\}$ pincer unit, **2a** was reacted with 0.5 equiv. of $[Cp^*IrCl_2]_2$ at low temperature (0–2 °C) to afford a mixture of $[Pt(XylNC)(\eta^5\text{-}Cp^*IrCl_2)(\mu\text{–}meso\text{-dpmppm}\text{–}\kappa^3,\kappa^1)](PF_6)_2$ (**6a**) and **5a** in ca. 3:1 ratio, which was monitored by ^1H and $^{31}P\{^1H\}$ NMR spectroscopy (Fig. S15a). Then, the mixture was treated with excess $BnNH_2$ at room temperature, and resulted in the formation of **5a** as a sole complex of *meso*-dpmppm (Fig. S15b); the NAC complex was not observed in the ^1H and $^{31}P\{^1H\}$ spectra. Complex **6a** was barely assigned by $^{31}P\{^1H\}$ spectroscopic techniques (Table 1 and Fig. S15a) with δ −51.5 (P_A: $^1J_{PtPA} = 1749$ Hz), −64.8 (P_B: $^1J_{PtPB} = 2260$ Hz), −0.5 (P_C), and −4.7 (P_D: $^1J_{PtPD} = 2174$ Hz) and $^2J_{PAPD} = 308$ Hz, in which $^1J_{PtPB}$ and $^2J_{PAPD}$ values are definitely close to those of **2a**, and the chemical shifts are alternatively similar to those of **5a**. Attachment of the $\{Cp^*IrCl_2\}$ fragment to the uncoordinated phosphine in **2a** caused a similar conformational change of the six-membered chelate ring from a stable chair conformation to a twist-boat structure in **6a**, which concomitantly reduced reactivity of the isocyanide ligand toward nucleophilic attack of the amine by steric hindrance of *meso*-dpmppm pincer ligand. These results could be interestingly recognized as on/off switching of the asymmetric $\{Pt^{II}(meso\text{-dpmppm}\text{–}\kappa^3)\}$ pincer complex induced by corporation of an additional Ir^I ligation (Fig. 5).

3. Conclusion

In the present study, the tetraphosphine *meso*-dpmppm (*meso*-bis[(diphenylphosphinomethyl)phenylphosphino]methane) proved to act as an asymmetric pincer ligand to Pt^{II} center in κ^3*PPP*-fashion, providing stable mononuclear Pt^{II} complexes, $[PtCl(meso\text{-dpmppm}\text{–}\kappa^3)]X$ (X = Cl (**1a**), PF_6 (**1b**)) and $[Pt(RNC)(meso\text{-dpmppm}\text{–}\kappa^3)](PF_6)_2$ (R = Xyl (**2a**), Cy (**2b**), ^{t}Bu (**2c**)). The isocyanide complexes **2a** and **2b** were treated with $R'NH_2$ (R = Bn, C_8H_{12}) and transformed to *N*-acyclic carbene complexes, $[Pt(meso\text{-dpmppm}\text{–}\kappa^3)\{C(NHR)(NHR')\}](PF_6)_2$ (R = Xyl, R' = Bn (**3a**), C_8H_{17} (**3b**); R = Cy, R' = Bn (**3c**)), while **2c** underwent N–C(^{t}Bu) bond cleavage upon heated with $R'NH_2$ (R' = Bn, *p*-Tol) to give $[Pt(C{\equiv}N)(meso\text{-dpmppm}\text{–}\kappa^3)]PF_6$ (**4**). The stereo-structures of **3** are influenced by the asymmetric structure of $\{Pt^{II}(meso\text{-dpmppm}\text{–}\kappa^3)\}$ unit, and the substituent groups of RNC and RNH_2. Interestingly, the reactivity of **2a** was entirely depressed by ligation of a $\{Cp^*IrCl_2\}$ fragment onto the uncoordinate phosphine of the pincer unit, through the conformational change of the six-membered [PtPCPCP] chelate ring from a stable chair form to a twist-boat form. In the latter structure, the axial site of Pt^{II} center is well protected sterically by phenyl groups of *meso*-dpmppm ligand, leading to on/off switching of the Pt^{II} pincer module. The present results provide useful information in relation to multifunctional asymmetric pincer-type ligand systems.

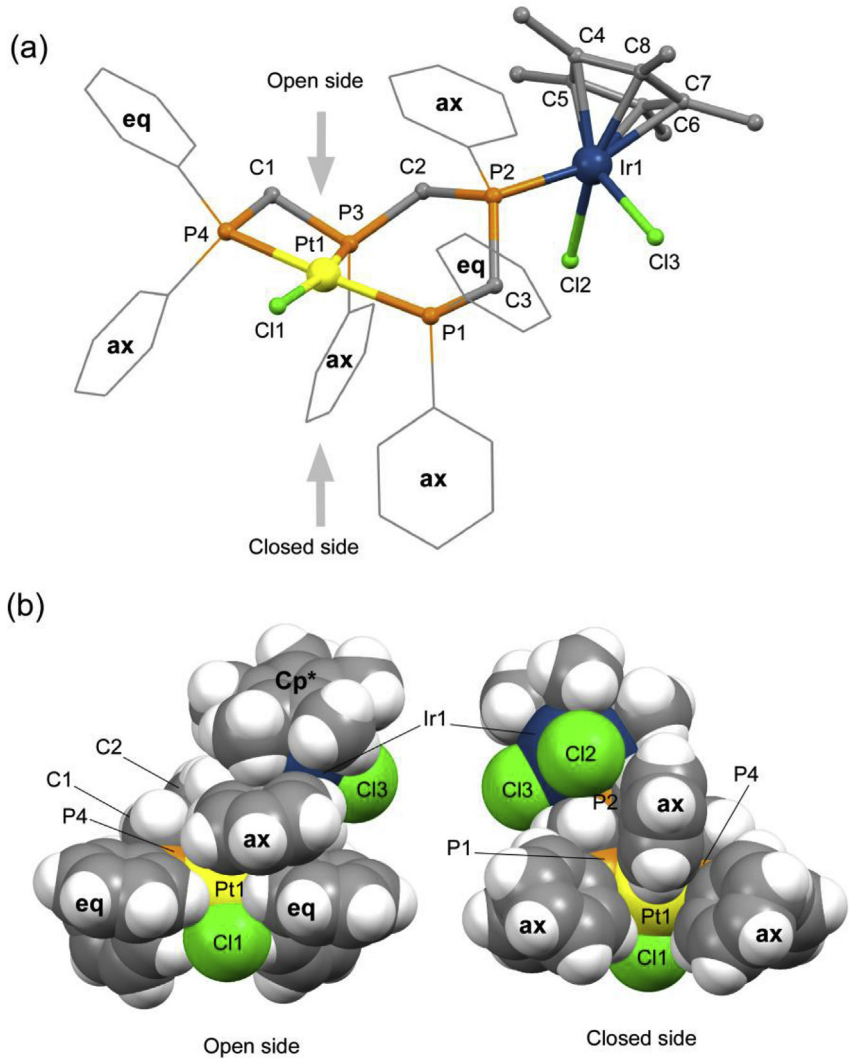

Fig. 4. (a) Perspective view for the complex cation of [PtCl(η^5–Cp*IrCl$_2$)(μ–*meso*-dpmppm–κ^3,κ^1)]PF_6 (**5a**), and (b) space-filling views for the complex cation of **5a** from Open side (left) and Closed side (right). **eq** indicates equatorially oriented phenyl groups of *meso*-dpmppm and **ax** indicates axially oriented ones.

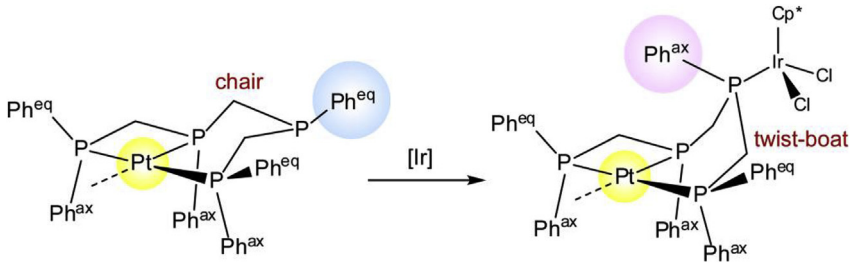

Fig. 5. Conformational change of {Pt^{II}(*meso*-dpmppm–κ^3)} asymmetric pincer unit induced by ligation of {Cp*IrCl$_2$} fragment onto the uncoordinate P atom. [Ir] = 0.5[Cp*IrCl$_2$]$_2$.

4. Experimental

4.1. General

All preparative procedures were carried out under nitrogen atmosphere using standard Schlenk techniques. All chemicals (highest purity available) were purchased from Wako Pure Chemical Industries, Ltd. Reagent grade solvents were dried by the standard procedures and were freshly distilled prior to their use. Compounds *meso*-dpmppm [8], [PtCl$_2$(cod)] [45], and [Cp*MCl$_2$]$_2$ (M = Ir, Rh) [46] were prepared by the methods described in the literature. ^{1}H and ^{1}H{^{31}P} NMR spectra were recorded on a Bruker AV-300N instrument (300 MHz) and the frequencies were referenced to the residual resonances of the deuterated solvent. ^{31}P{^{1}H} NMR spectra were recorded on the same instrument at 121 MHz with chemical shifts being calibrated to 85% H_3PO_4 as an external reference. The assignments of ^{31}P NMR, P_A, P_B, P_C, and P_D are shown in Table 1. Electronic absorption spectra were recorded on a JASCO

UV600 spectrophotometer at room temperatures. IR spectra of solid samples as KBr disks were recorded on a JASCO FT/IR-410 spectrophotometer at ambient temperature. ESI-TOF mass spectra were recorded on a JEOL JMS-T100LC in a positive detection mode in the range of *m/z* 100–3000, equipped with an ion spray interface. The sprayer was held at a potential of +2.0 kV, and the compressed N_2 was employed to assist liquid nebulization.

4.2. Preparation of [PtCl(meso-dpmppm–κ^3)]Cl (**1a**)

To a solution of *meso*-dpmppm (45 mg, 0.072 mmol) in dichloromethane (5 mL) was added [$PtCl_2$(cod)] (27 mg, 0.072 mmol), and the reaction mixture was stirred at room temperature for 3 h. The solvent was removed under reduced pressure to dryness and the residue was washed with diethyl ether (5 mL) and crystallized from a dichloromethane (3 mL)/diethyl ether (3 mL) mixed solvent, with allowing to stand in a refrigerator, to give colorless crystals of **1a**·3.5CH_2Cl_2, which were collected by filtration, washed with diethyl ether, and dried under vacuum (44 mg, 51%). Anal. Calc. for $C_{42.5}H_{43}P_4Cl_9Pt$ (**1a**·3.5CH_2Cl_2 (1191.846)): C, 42.83; H, 3.64. Found: C, 42.47; H, 3.57. IR (KBr): ν 1483 (m), 1436 (s), 1100 (s), 1048 (m), 1027 (m), 745 (s), 712 (m), 692 (s), 490 (s) cm^{-1}. $^1H\{^{31}P\}$ NMR ($CDCl_3$): δ 2.61 (d, 1H, C*H*$_2$), 2.77 (d, 1H, C*H*$_2$), 3.89 (d, 1H, C*H*$_2$), 4.76 (d, 1H, C*H*$_2$), 4.99 (d, 1H, C*H*$_2$), 5.48 (d, 1H, C*H*$_2$), 6.95–7.98 (m, 30H, Ar*H*). $^{31}P\{^1H\}$ NMR ($CDCl_3$): δ −47.7 (ddd, 1P (P_B), $J_{PP'}$ = 69, 68, 15 Hz, $^1J_{PtP}$ = 2831 Hz), −39.6 (dd, 1P (P_C), $J_{PP'}$ = 69, 46 Hz), −36.7 (dd, 1P (P_A), $J_{PP'}$ = 419, 68 Hz, $^1J_{PtP}$ = 1992 Hz), 3.9 (ddd, 1P (P_D), $J_{PP'}$ = 419, 46, 15 Hz, $^1J_{PtP}$ = 2503 Hz). ESI–MS ($CHCl_3$): *m/z* 859.185 (*z*1, $[PtCl(dpmppm)]^+$ (859.111)).

4.3. Preparation of [PtCl(meso-dpmppm-κ^3)]PF_6 (**1b**)

To a dichloromethane solution (10 mL) containing dpmppm (105 mg, 0.167 mmol) was added [$PtCl_2$(cod)] (63 mg, 0.167 mmol) and NH_4PF_6 (138 mg, 0.843 mmol). The mixture was stirred at room temperature overnight. The solution was concentrated under reduced pressure to dryness and the residue was washed with diethyl ether (5 mL) and extracted with 5 mL of CH_2Cl_2. The solution was passed through a membrane filter and concentrated to ca. 3 mL to which diethyl ether (ca. 0.5 mL) was added carefully. The solution was allowed to stand in refrigerator to afford colorless crystals of **1b** (127 mg, 76%). Anal. Calc. for $C_{39}H_{36}P_5ClF_6Pt$ (**1b** (1004.093)): C, 46.65; H, 3.61. Found: C, 46.21; H, 3.48. IR (KBr): ν 1484 (m), 1438 (s), 1379 (w), 1309 (w), 1107 (s), 1041 (m), 1025 (m), 999 (m), 836 (s), 741 (s), 712 (m), 690 (s), 557 (s), 515 (m), 492 (s) cm^{-1}. $^1H\{^{31}P\}$ NMR (acetone-d_6): δ 3.26–3.50 (m, 3H, C*H*$_2$), 3.73 (d, 1H, C*H*$_2$), 4.74 (d, 1H, C*H*$_2$), 5.38 (d, 1H, C*H*$_2$), 7.21–8.28 (m, 30H, Ar*H*). $^{31}P\{^1H\}$ NMR (acetone-d_6): δ −144.1 (sep, 1P, PF_6, $^1J_{PF}$ = 708 Hz), −51.5 (ddd, 1P (P_B), $J_{PP'}$ = 70, 67, 14 Hz, $^1J_{PtP}$ = 2721 Hz), −40.0 (dd, 1P (P_C), $J_{PP'}$ = 70, 45 Hz), −40.2 (dd, 1P (P_A), $J_{PP'}$ = 419, 67 Hz, $^1J_{PtP}$ = 1956 Hz), 6.0 (ddd, 1P (P_D), $J_{PP'}$ = 419, 45, 14 Hz, $^1J_{PtP}$ = 2466 Hz). ESI–MS (acetone): *m/z* 859.202 (*z*1, $[PtCl(dpmppm)]^+$ (859.111)).

4.4. Preparation of [Pt(dpmppm–κ^3)(XylNC)]$(PF_6)_2$ (**2a**)

To a CH_2Cl_2 solution (5 mL) containing *meso*-dpmppm (49 mg, 0.078 mmol) were added [$PtCl_2$(cod)] (30 mg, 0.079 mmol), XylNC (13 mg, 0.096 mmol), and NH_4PF_6 (64 mg, 0.40 mmol) with 5 mL of acetone. The mixture was stirred at room temperature for 12 h, and then, the solvent was evaporated under reduced pressure to dryness. The residue was washed with Et_2O (5 mL x 4) and extracted with CH_2Cl_2 (10 mL). The extract was passed through a glass filter and concentrated to ca. 3 mL. After careful addition of Et_2O (2.5 mL), the solution was allowed to stand in refrigerator to afford colorless crystals of **2a**·0.5CH_2Cl_2·0.5Et_2O, which were separated by filtration, washed with Et_2O, and dried under vacuum (49 mg, yield 47%). Anal. Calc. for $C_{50.5}H_{51}O_{0.5}NP_6ClF_{12}Pt$ (**2a**·0.5CH_2Cl_2·0.5Et_2O (1324.306)): C, 45.80; H, 3.88; N, 1.06. Found: C, 45.78; H, 3.91; N, 1.15. IR (KBr): ν 2200 (s, N≡C), 1484 (m), 1438 (s, P–C), 1106 (s), 999 (m), 840 (s, PF_6), 779 (m), 744 (m), 711 (m), 691 (m), 558 (s) cm^{-1}. $^1H\{^{31}P\}$ NMR (CD_2Cl_2): δ 1.52 (s, 6H, *o*-C*H*$_3$), 2.68 (d, 1H, C*H*$_2$), 2.91 (d, 1H, C*H*$_2$), 3.63 (d, 1H, C*H*$_2$), 3.70 (d, 1H, C*H*$_2$), 4.74 (d, 1H, C*H*$_2$), 5.09 (d, 1H, C*H*$_2$), 6.87–7.99 (m, 36H, Ar*H*). $^{31}P\{^1H\}$ NMR (CD_2Cl_2): δ −144.4 (sep, 2P, PF_6, $^1J_{PF}$ = 714 Hz), −50.0 (ddd, 1P, P_B, $J_{PP'}$ = 73, 69, 19 Hz, $^1J_{PtP}$ = 2308 Hz), −42.0 (dd, 1P, P_C, $J_{PP'}$ = 73, 36 Hz), −36.2 (dd, 1P, P_A, $J_{PP'}$ = 322, 69 Hz, $^1J_{PtP}$ = 1774 Hz), −1.0 (ddd, 1P, P_D, $J_{PP'}$ = 322, 36, 19 Hz, $^1J_{PtP}$ = 2248 Hz). ESI–MS (acetone): *m/z* 953.291 (*z*1, $\{Pt(dpmppm)(XylNC) - H\}^+$ (953.208)), 1099.275 (*z*1, $\{[Pt(dpmppm)(XylNC)]PF_6\}^+$ (1099.180)).

4.5. Preparation of [Pt(dpmppm–κ^3)(CyNC)]$(PF_6)_2$ (**2b**)

By a procedure similar to **2a**, colorless crystals of **2b**·0.25CH_2Cl_2 were obtained in 68% yield (66 mg) from *meso*-dpmppm (50 mg, 0.079 mmol), [$PtCl_2$(cod)] (29 mg, 0.078 mmol), CyNC (11 μL, 0.094 mmol), and NH_4PF_6 (65 mg, 0.40 mmol). Anal. Calc. for $C_{46.25}H_{47.5}NP_6Cl_{0.5}F_{12}Pt$ (**2b**·0.25CH_2Cl_2 (1244.007)): C, 44.65; H, 3.85; N, 1.13. Found: C, 44.61; H, 3.61; N, 1.30. IR (KBr): ν 2238 (s, N≡C), 1485 (m), 1438 (s, P–C), 1106 (m), 838 (s, PF_6), 743 (m), 712 (m), 691 (m), 558 (s), 490 (m) cm^{-1}. $^1H\{^{31}P\}$ NMR (CD_2Cl_2): δ 1.06–1.38 (m, 11H, *Cy*), 2.69 (d, 1H, C*H*$_2$), 2.96 (d, 3H, C*H*$_2$), 3.70 (d, 1H, C*H*$_2$), 3.75 (d, 1H, C*H*$_2$), 4.78 (d, 1H, C*H*$_2$), 5.08 (d, 1H, C*H*$_2$), 7.12–8.00 (m, 30H, Ar*H*). $^{31}P\{^1H\}$ NMR (CD_2Cl_2): δ −144.4 (sep, 2P, PF_6, $^1J_{PF}$ = 714 Hz), −50.6 (ddd, 1P, P_B, $J_{PP'}$ = 109, 63, 18 Hz, $^1J_{PtP}$ = 2296 Hz), −41.7 (dd, 1P, P_C, $J_{PP'}$ = 109, 61 Hz), −36.0 (dd, 1P, P_A, $J_{PP'}$ = 316, 63 Hz, $^1J_{PtP}$ = 1774 Hz), −1.5 (ddd, 1P, P_D, $J_{PP'}$ = 316, 61, 18 Hz, $^1J_{PtP}$ = 2260 Hz). ESI–MS (acetone): *m/z* 931.332 (*z*1, $\{Pt(dpmppm)(CyNC) - H\}^+$ (931.223)), 1077.325 (*z*1, $\{[Pt(dpmppm)(CyNC)]PF_6\}^+$ (1077.195)).

4.6. Preparation of [Pt(dpmppm–κ^3)(^{t}BuNC)]$(PF_6)_2$ (**2c**)

By a procedure similar to **2a**, colorless crystals of **2c**·0.25CH_2Cl_2 were obtained in 59% yield (58 mg) from *meso*-dpmppm (51 mg, 0.081 mmol), [$PtCl_2$(cod)] (30 mg, 0.081 mmol), ^{t}BuNC (11 μL, 0.097 mmol), and NH_4PF_6 (65 mg, 0.40 mmol). Anal. Calc. for $C_{44.25}H_{45.5}NP_6Cl_{0.5}F_{12}Pt$ (**2c**·0.25CH_2Cl_2 (1217.969)): C, 43.64; H, 3.77; N, 1.15. Found: C, 43.57; H, 3.84; N, 1.22. IR (KBr): ν 2234 (s, N≡C), 1485 (m), 1438 (s, P–C), 1106 (m), 841 (s, PF_6), 744 (m), 713 (m), 691 (m), 558 (s), 491 (m) cm^{-1}. $^1H\{^{31}P\}$ NMR (CD_2Cl_2): δ 0.94 (s, 9H, ^{t}*Bu*), 2.69 (d, 1H, C*H*$_2$), 2.96 (d, 3H, C*H*$_2$), 3.73 (d, 1H, C*H*$_2$), 3.75 (d, 1H, C*H*$_2$), 4.79 (d, 1H, C*H*$_2$), 5.03 (d, 1H, C*H*$_2$), 7.16–8.00 (m, 30H, Ar*H*). $^{31}P\{^1H\}$ NMR (CD_2Cl_2): δ −144.3 (sep, 2P, PF_6, $^1J_{PF}$ = 714 Hz), −50.4 (ddd, 1P, P_B, $J_{PP'}$ = 85, 69, 18 Hz, $^1J_{PtP}$ = 2272 Hz), −41.7 (dd, 1P, P_C, $J_{PP'}$ = 85, 49 Hz), −36.2 (dd, 1P, P_A, $J_{PP'}$ = 322, 69 Hz, $^1J_{PtP}$ = 1749 Hz), −1.7 (ddd, 1P, P_D, $J_{PP'}$ = 322, 49, 18 Hz, $^1J_{PtP}$ = 2260 Hz). ESI–MS (acetone): *m/z* 905.305 (*z*1, $\{Pt(dpmppm)(^tBuNC) - H\}^+$ (905.208)), 1051.282 (*z*1, $\{[Pt(dpmppm)(^tBuNC)]PF_6\}^+$ (1051.180)).

4.7. Preparation of [Pt(dpmppm–κ^3){C(NHXyl)(NHBn)}]$(PF_6)_2$ (**3a**)

To a dichloromethane solution (5 mL) containing **2a**·0.5CH_2Cl_2·0.5Et_2O (21 mg, 0.016 mmol) was added excess of $BnNH_2$ (7.3 μL, 0.067 mmol), and the solution was stirred at room temperature for 12 h. The solvent was evaporated under reduced pressure to dryness, and the residue was washed with Et_2O (5 mL x 4) and extracted with CH_2Cl_2 (10 mL). The extract was passed through a glass filter and concentrated to 3 mL. After careful addition of Et_2O (2.5 mL), the solution was allowed to stand in refrigerator to afford colorless crystals of **3a**·0.25CH_2Cl_2, which were separated by filtration, washed with Et_2O, and dried under

vacuum (12 mg, yield 54%). Anal. Calc. for $C_{55.25}H_{54.5}N_2P_6Cl_{0.5}F_{12}Pt$ (**3a**·0.25CH_2Cl_2 (1373.165)): C, 48.33; H, 4.00; N, 2.04. Found: C, 48.30; H, 3.86; N, 2.07. IR (KBr): ν 3386, 3314 (m, NH), 1546 (s, N=C), 1485 (m), 1438 (s, P–C), 1101 (s), 999 (m), 843 (s, PF_6), 776 (m), 742 (m), 712 (m), 692 (m), 558 (s) cm^{-1}. $^1H\{^{31}P\}$ NMR (CD_2Cl_2): δ 1.81 (s, 3H, *o*-CH_3), 1.86 (s, 3H, *o*-CH_3), 2.52 (d, 1H, CH_2), 2.85 (d, 1H, CH_2), 3.63 (d, 1H, CH_2), 3.82 (d, 1H, CH_2), 3.97 (d, 1H, CH_2), 4.09 (d, 1H, CH_2), 4.79 (d, 1H, NCH_2Ph), 5.85 (s, 1H, N*H*CH_2Ph), 6.08 (d, 1H, NCH_2Ph), 6.90–8.11 (m, 38H, Ar*H*), 8.69 (s, 1H, N*H*Xyl). $^{31}P\{^1H\}$ NMR (CD_2Cl_2): δ −144.3 (sep, 2P, PF_6, $^1J_{PF} = 714$ Hz), −47.3 (ddd, 1P, P_B, $J_{PP'} = 85$, 55, 19 Hz, $^1J_{PtP} = 1664$ Hz), −46.9 (dd, 1P, P_C, $J_{PP'} = 85$, 61 Hz), −36.2 (dd, 1P, P_A, $J_{PP'} = 340$, 55 Hz, $^1J_{PtP} = 2017$ Hz), −2.2 (ddd, 1P, P_D, $J_{PP'} = 340$, 61, 19 Hz, $^1J_{PtP} = 2515$ Hz). ESI–MS (acetone): *m/z* 530.648 (*z*2, [Pt(dpmppm){C(NHXyl)(NHBn)}]$^{2+}$ (530.645)), 1060.324 (*z*1, {Pt(dpmppm){C(NHXyl)(NHBn)} − H}$^+$ (1060.281)), 1206.305 (*z*1, {[Pt(dpmppm){C(NHXyl)(NHBn)}]PF_6}$^+$ (1206.253)).

4.8. Preparation of [Pt(dpmppm−κ^3){C(NHXyl)(NHC_8H_{17})}](PF_6)$_2$ (**3b**)

To a dichloromethane solution (5 mL) containing **2a**·0.5CH_2Cl_2·0.5Et_2O (18 mg, 0.014 mmol) was added excess of *n*-octylamine ($C_8H_{17}NH_2$) (9.5 μL, 0.057 mmol), and the solution was stirred at room temperature for 12 h. The solvent was evaporated under reduced pressure to dryness, and the residue was washed with Et_2O (5 mL x 2) and extracted with CH_2Cl_2 (5 mL). The extract was passed through a glass filter and concentrated to 3 mL. After careful addition of Et_2O (2.5 mL), the solution was allowed to stand in refrigerator to afford colorless crystals of **3b**, which were separated by filtration, washed with Et_2O, and dried under vacuum (9.1 mg, yield 49%). Anal. Calc. for $C_{56}H_{64}N_2P_6F_{12}Pt$ (**3b** (1374.022)): C, 48.95; H, 4.69; N, 2.04. Found: C, 48.68; H, 4.29; N, 2.02. IR (KBr): ν 3386, 3298 (m, NH), 1561 (s, N=C), 1485 (m), 1438 (s, P–C), 1099 (s), 1000 (m), 845 (s, PF_6), 777 (m), 744 (m), 712 (m), 693 (m), 558 (s) cm^{-1}. $^1H\{^{31}P\}$ NMR (CD_2Cl_2): δ 0.04–1.26 (m, 17H, C_8H_{17}), 1.82 (s, 3H, *o*-CH_3), 1.89 (s, 3H, *o*-CH_3), 2.60 (d, 1H, CH_2), 2.90 (d, 1H, CH_2), 3.71 (d, 1H, CH_2), 4.05 (d, 1H, CH_2), 4.82 (d, 1H, CH_2), 4.94 (d, 1H, CH_2), 5.57 (s, 1H, N*H*C_8H_{17}), 7.01–8.15 (m, 33H, Ar*H*), 8.58 (s, 1H, N*H*Xyl). $^{31}P\{^1H\}$ NMR (CD_2Cl_2): δ −143.9 (sep, 2P, PF_6, $^1J_{PF} = 714$ Hz), −47.1 (ddd, 1P, P_B, $J_{PP'} = 85$, 60, 19 Hz, $^1J_{PtP} = 1689$ Hz), −46.0 (dd, 1P, P_C, $J_{PP'} = 85$, 61 Hz), −35.9 (dd, 1P, P_A, $J_{PP'} = 340$, 60 Hz, $^1J_{PtP} = 2138$ Hz), −1.0 (ddd, 1P, P_D, $J_{PP'} = 340$, 61, 19 Hz, $^1J_{PtP} = 2527$ Hz). ESI–MS (acetone): *m/z* 541.302 (*z*2, [Pt(dpmppm){C(NHXyl)(NHC_8H_{17})}]$^{2+}$ (541.684)), 1228.471 (*z*1, {[Pt(dpmppm){C(NHXyl)(NHC_8H_{17})}]PF_6}$^+$ (1228.331)).

4.9. Preparation of [Pt(dpmppm−κ^3){C(NHCy)(NHBn)}](PF_6)$_2$ (**3c**)

To a dichloromethane solution (5 mL) containing **2b**·0.25CH_2Cl_2 (19 mg, 0.015 mmol) was added excess of $BnNH_2$ (6.7 μL, 0.061 mmol), and the solution was stirred at room temperature for 12 h. The work-up similar to that of **3a** afford colorless crystals of **3c**·0.25CH_2Cl_2 (9.1 mg, yield 45%). Anal. Calc. for $C_{53.25}H_{56.5}N_2P_6Cl_{0.5}F_{12}Pt$ (**3c**·0.25CH_2Cl_2 (1351.160)): C, 47.33; H, 4.21; N, 2.07. Found: C, 47.46; H, 3.96; N, 2.17. IR (KBr): ν 3395, 3341 (m, NH), 1570 (s, N=C), 1485 (m), 1438 (s, P–C), 1102 (s), 999 (w), 845 (s, PF_6), 774 (w), 743 (m), 713 (m), 692 (m), 558 (s) cm^{-1}. $^1H\{^{31}P\}$ NMR (CD_2Cl_2): δ 0.95–1.65 (m, 11H, Cy), 2.80–3.98 (m, 4H, CH_2), 4.62 (d, 1H, CH_2), 6.20 (br s, 2H, N*H*Bn/N*H*Cy), 6.40 (d, 1H, NCH_2Ph), 7.17 (d, 1H, NCH_2Ph), 7.21–8.01 (m, 35H, Ar*H*). $^{31}P\{^1H\}$ NMR (CD_2Cl_2): major: minor = 1.2: 1, δ(major) −144.1 (sep, 2P, PF_6, $^1J_{PF} = 715$ Hz), −48.6 (ddd, 1P, P_B, $J_{PP'} = 82$, 59, 23 Hz, $^1J_{PtP} = 1582$ Hz), −42.8 (dd, 1P, P_C, $J_{PP'} = 83$, 66 Hz), −29.3 (dd, 1P, P_A, $J_{PP'} = 337$, 59 Hz, $^1J_{PtP} = 2017$ Hz), 3.2 (ddd, 1P, P_D, $J_{PP'} = 337$, 66, 23 Hz, $^1J_{PtP} = 2478$ Hz); δ(minor) −144.1 (sep, 2P, PF_6, $^1J_{PF} = 715$ Hz), −48.8 (ddd, 1P, P_B, $J_{PP'} = 83$, 59, 23 Hz, $^1J_{PtP} = 1582$ Hz), −43.8 (dd, 1P, P_C, $J_{PP'} = 83$, 66 Hz), −30.2 (dd, 1P, P_A, $J_{PP'} = 337$, 59 Hz, $^1J_{PtP} = 2017$ Hz), 2.3 (ddd, 1P, P_D, $J_{PP'} = 337$, 66, 23 Hz, $^1J_{PtP} = 2478$ Hz). ESI–MS (acetone): *m/z* 519.656 (*z*2, [Pt(dpmppm){C(NHCy)(NHBn)}]$^{2+}$ (519.652)), 1038.318 (*z*1, {Pt(dpmppm){C(NHCy)(NHBn)}−H}$^+$ (1038.297)), 1184.290 (*z*1, {[Pt(dpmppm){C(NHCy)(NHBn)}]PF_6}$^+$ (1184.269)). Single crystals of **3c**·Et_2O·$(CH_3)_2CO$ suitable for X-ray crystallography were obtained by recrystallization from an acetone/diethyl ether mixed solvent.

4.10. Preparation of [Pt(CN)(dpmppm−κ^3)]PF_6 (**4**)

To a dichloromethane solution (5 mL) containing **2c**·0.25CH_2Cl_2 (9.4 mg, 0.0077 mmol) was added *p*-toluidine (*p*-TolNH_2) (3.4 mg, 0.032 mmol), and the solution was stirred at 80 °C for 12 h. The solvent was evaporated under reduced pressure to dryness, and the residue was washed with Et_2O (5 mL x 4) and extracted with CH_2Cl_2 (5 mL). The extract was passed through a glass filter and concentrated to 3 mL. After careful addition of Et_2O (2.5 mL), the solution was allowed to stand in refrigerator to afford pale yellow crystals of **4** (5.1 mg, yield 67%). Anal. Calc. for $C_{40}H_{36}NP_5F_6Pt$ (**4** (994.658)): C, 48.30; H, 3.65; N, 1.41. Found: C, 47.98; H, 3.57; N, 1.52. IR (KBr): ν 2147 (s, NC), 1485 (m), 1438 (s, P–C), 1106 (s), 999 (m), 838 (s, PF_6), 778 (m), 743 (m), 713 (m), 692 (m), 558 (s) cm^{-1}. $^1H\{^{31}P\}$ NMR (CD_2Cl_2): δ 2.76 (d, 1H, CH_2), 2.86 (d, 1H, CH_2), 3.13 (d, 1H, CH_2), 3.27 (d, 1H, CH_2), 4.57 (d, 1H, CH_2), 5.11 (d, 1H, CH_2), 7.03–8.00 (m, 30H, Ar*H*). $^{31}P\{^1H\}$ NMR (CD_2Cl_2): δ −144.1 (sep, 2P, PF_6, $^1J_{PF} = 713$ Hz), −54.0 (ddd, 1P, P_B, $J_{PP'} = 85$, 62, 19 Hz, $^1J_{PtP} = 2005$ Hz), −39.4 (dd, 1P, P_C, $J_{PP'} = 85$, 49 Hz), −37.8 (dd, 1P, P_A, $J_{PP'} = 352$, 62 Hz, $^1J_{PtP} = 1907$ Hz), 0.3 (ddd, 1P, P_D, $J_{PP'} = 352$, 49, 19 Hz, $^1J_{PtP} = 2369$ Hz). ESI–MS (acetone): *m/z* 849.204 (*z*1, [Pt(CN)(dpmppm)]$^+$ (849.145)).

4.11. Preparation of [PtCl(η^5−Cp*MCl_2)(μ−*meso*-dpmppm−κ^3,κ^1)]PF_6 (M = Ir (**5a**), Rh (**5b**))

Compound **1b** (39 mg, 0.039 mmol) was treated with $[Cp^*IrCl_2]_2$ (16 mg, 0.020 mmol) in dichloromethane (5 mL) and the solution was stirred at room temperature overnight. The solvent was removed under reduced pressure and the residue was extracted with 10 mL of dichloromethane which was passed through a membrane filter. The extract was concentrated to ca. 2 mL and diethyl ether (ca. 3.5 mL) was added to the solution slowly. The solution was allowed to stand in refrigerator to afford orange crystals of **5a**, which were collected and dried under vacuum (42 mg, 77%). Anal. Calc. for $C_{49}H_{51}F_6P_5Cl_3PtIr$ (**5a** (1402.442)): C, 41.96; H, 3.67. Found: C, 41.65; H, 3.64. IR (KBr): ν 1436 (s, P–C), 1100 (m), 840 (s, PF_6), 795 (m), 741 (m), 690 (m), 557 (m), 530 (m) cm^{-1}. UV–vis (CH_2Cl_2): λ_{max} (log ε) 361^{sh} (3.45), 438 (2.74) nm. $^1H\{^{31}P\}$ NMR (CD_2Cl_2): δ 1.40 (s, 15H, Cp*), 2.96 (d, 1H, CH_2), 3.56 (d, 1H, CH_2), 3.93 (d, 1H, CH_2), 4.83 (d, 1H, CH_2), 4.94 (d, 1H, CH_2), 5.36 (d, 1H, CH_2), 6.87–8.22 (m, 30H, Ar*H*). $^{31}P\{^1H\}$ NMR (CD_2Cl_2): δ −144.2 (sep, $^1J_{PF} = 713$ Hz, 1P, PF_6), −60.4 (ddd, 1P (P_B), $J_{PP'} = 62$, 26, 11 Hz, $^1J_{PtP} = 2770$ Hz), −52.6 (dd, 1P (P_A), $J_{PP'} = 401$, 62 Hz, $^1J_{PtP} = 1907$ Hz), −9.5 (ddd, 1P (P_D), $J_{PP'} = 401$, 21, 11 Hz, $^1J_{PtP} = 2381$ Hz), −1.9 (dd, 1P (P_C), $J_{PP'} = 26$, 21 Hz). ESI–MS (acetone): *m/z* 1257.235 (*z*1, [PtCl(dpmppm)(Cp^*IrCl_2)]$^+$ (1257.127)).

Portions of **1b** (41 mg, 0.041 mmol) and $[Cp^*RhCl_2]_2$ (12.5 mg, 0.020 mmol) were dissolved in dichloromethane (5 mL) and the solution was stirred at room temperature overnight. The solvent was removed under reduced pressure and the residue was extracted with 5 mL of dichloromethane which was passed through a membrane filter. The extract was concentrated to ca. 3 mL and diethyl ether (ca. 2 mL) was added to the solution slowly. The solution was allowed to stand in refrigerator to afford orange crystals of **5b**, which were collected and dried under vacuum (33 mg, 62%). Anal. Calc. for $C_{49}H_{51}F_6P_5Cl_3PtRh$ (**5b** (1313.131)): C, 44.82; H, 3.91%. Found: C, 44.67; H, 3.66%. IR (KBr): ν 1436 (s, P–C), 1099 (m), 1048 (m), 839 (s, PF_6), 740 (m), 690 (m), 557 (m), 528 (m), 502 (m), 474

Table 2
Crystallographic data of **1a,b**, **2a-c**, **3a-c**, **4**, and **5a,b**.

Compound	**1a**·$2CH_2Cl_2$	**1b**	**2a**·$3CH_2Cl_2$	**2b**·$2CH_2Cl_2$	**2c**·$2CH_2Cl_2$
formula	$C_{41}H_{40}Cl_6P_4Pt$	$C_{39}H_{36}ClF_6P_5Pt$	$C_{51}H_{51}Cl_6F_{12}N\ P_6Pt$	$C_{48}H_{51}Cl_4F_{12}NP_6Pt$	$C_{46}H_{49}Cl_4F_{12}N\ P_6Pt$
formula wt	1064.47	1004.12	1499.60	1392.66	1366.63
cryst. syst	monoclinic	orthorhombic	triclinic	monoclinic	monoclinic
space group	$P2_1/c$	$P2_12_12_1$	$P\bar{1}$	$P2_1/n$	$P2_1/n$
a, Å	11.1569(4)	13.676(5)	10.850(3)	11.9653(8)	11.732(3)
b, Å	29.7495(11)	16.086(5)	12.899(3)	20.2897(11)	20.366(5)
c, Å	13.232(5)	18.253(6)	22.667(6)	23.6238(19)	23.416(6)
α, deg	90	90	82.911(8)	90	90
β, deg	96.8543(16)	90	83.647(9)	104.425(3)	101.751(3)
γ, deg	90	90	60.092(7)	90	90
V, Å^3	4360.5(3)	4015(2)	2933.2(12)	5554.4(7)	5578(2)
Z	4	4	2	4	4
*R*1[a]	0.033	0.034	0.086	0.032	0.038
*wR*2[b]	0.074	0.068	0.218	0.077	0.091
GOF	1.158	0.969	1.107	1.023	1.072

Compound	**3a**·$0.5CH_2Cl_2$	**3b**	**3c**·Et_2O·$(CH_3)_2CO$	**4**	**5a**·$3CH_2Cl_2$	**5b**·$3CH_2Cl_2$
formula	$C_{55.5}H_{55}ClF_{12}N_2P_6Pt$	$C_{56}H_{64}F_{12}N_2P_6Pt$	$C_{60}H_{72}F_{12}N_2O_2P_6Pt$	$C_{40}H_{36}F_6NP_5Pt$	$C_{52}H_{57}Cl_9F_6P_5PtIr$	$C_{52}H_{57}Cl_9F_6P_5PtRh$
formula wt	1394.43	1374.05	1462.15	994.68	1657.27	1567.95
cryst. syst	triclinic	monoclinic	triclinic	orthorhombic	triclinic	triclinic
space group	$P\bar{1}$	$C2/c$	$P\bar{1}$	$P2_12_12_1$	$P\bar{1}$	$P\bar{1}$
a, Å	13.163(2)	27.060(5)	12.276(4)	13.615(5)	12.410(3)	12.385(6)
b, Å	16.043(2)	21.296(3)	14.099(4)	16.306(6)	14.535(4)	14.534(8)
c, Å	17.732(3)	23.171(4)	18.642(6)	18.407(7)	17.799(5)	17.832(9)
α, deg	72.490(7)	90	85.778(6)	90	80.907(8)	80.894(12)
β, deg	80.626(8)	94.781(2)	82.731(6)	90	75.596(9)	75.583(13)
γ, deg	71.786(7)	90	85.222(6)	90	79.429(7)	79.588(13)
V, Å^3	3382.3(9)	13306(4)	3183.0(16)	4086(3)	3035.6(14)	3036(3)
Z	2	8	2	4	2	2
*R*1[a]	0.061	0.058	0.088	0.044	0.036	0.034
*wR*2[b]	0.188	0.164	0.249	0.106	0.093	0.082
GOF	1.085	1.079	1.072	1.100	1.067	0.976

[a] $R1 = \Sigma||F_o| - |F_c||/\Sigma|F_o|$ (for obsd. refs with $I > 2\sigma(I)$).
[b] $wR2 = [\Sigma w(F_o^2 - F_c^2)^2/\Sigma w(F_o^2)^2]^{1/2}$ (for all refs).

(m) cm^{-1}. UV–vis (CH_2Cl_2): λ_{max} (log ε) 399 (3.65) nm. $^1H\{^{31}P\}$ NMR (CD_2Cl_2): δ 1.39 (s, 15H, Cp*), 2.96 (d, 1H, CH_2), 3.56 (d, 1H, CH_2), 3.93 (d, 1H, CH_2), 4.83 (d, 1H, CH_2), 4.94 (d, 1H, CH_2), 5.38 (d, 1H, CH_2), 6.88–8.22 (m, 30H, Ar*H*). $^{31}P\{^1H\}$ NMR (CD_2Cl_2): δ −144.2 (sep, $^1J_{PF} = 713$ Hz, 1P, PF_6), −60.0 (ddd, 1P (P_B), $J_{PP'} = 61$, 32, 10 Hz, $^1J_{PtP} = 2770$ Hz, $^3J_{RhP} = 5$ Hz), −52.5 (dd, 1P (P_A), $J_{PP'} = 413$, 61 Hz, $^1J_{PtP} = 1944$ Hz), −8.9 (ddd, 1P (P_D), $J_{PP'} = 413$, 27, 10 Hz, $^1J_{PtP} = 2381$ Hz, $^3J_{RhP} = 4$ Hz), 30.2 (ddd, 1P (P_C), $J_{PP'} = 32$, 27 Hz, $^1J_{RhP} = 149$ Hz). ESI–MS (acetone): *m/z* 1167.128 (*z*1, $[PtCl(dpmppm)(Cp^*RhCl_2)]^+$ (1167.070)).

4.12. X-ray crystallographic analysis

The crystals of **1a**·$2CH_2Cl_2$, **1b**, **2a**·$3CH_2Cl_2$, **2b**·$2CH_2Cl_2$, **2c**·$2CH_2Cl_2$, **3a**·$0.5CH_2Cl_2$, **3b**, **3c**·Et_2O·$(CH_3)_2CO$, **4**, **5a**·$3CH_2Cl_2$, and **5b**·$3CH_2Cl_2$ were quickly coated with Paratone N oil and mounted on top of a loop fiber at room temperature. Crystal and experimental data are summarized in Table 2 and Tables S1–S4. All data were collected at −120 °C on a Rigaku AFC8R/Mercury CCD diffractometer equipped with graphite-monochromated Mo Kα radiation using a rotating-anode X-ray generator (50 kV, 180 mA) and a Rigaku VariMax Mo/Saturn CCD diffractometer equipped with graphite-monochromated Mo Kα radiation using a rotating-anode X-ray generator RA-Micro 7 (50 kV, 24 mA). A total of 720–2160 oscillation images, covering a whole sphere of 6° < 2θ < 55° were corrected by the ω–scan method (−70° < ω < 110° (**1b** and **3a**,**b**), −62° < ω < 118° (**1a**, **2a-c**, **3c**, **4**, and **5a**,**b**)) with Δω of 0.25° or 0.50°. The crystal-to-detector (70 × 70 mm) distance was set at 45 or 60 mm. The data were processed using the *Crystal Clear 1.3.5* program (Rigaku/MSC) [47] and corrected for Lorentz–polarization and absorption effects [48] The structures of complexes were solved by direct methods with *SHELXLS-97* [49] (**5a**) and SIR-97 [50] (**1a,b**, **2a-c**, **3a-c**, **4**, and **5b**), and were refined on F^2 with full-matrix least-squares techniques with *SHELXL-97* [49] using *Crystal Structure 4.0* package [51]. All non-hydrogen atoms were refined with anisotropic thermal parameters, and the C–H hydrogen atoms were calculated at ideal positions and refined with riding models. All calculations were carried out on a Windows PC with *Crystal Structure 4.0* package [51]. In the refinement of **3a**, the N–H hydrogen atoms were determined from difference Fourier maps and refined with riding models. The final residual electron densities in a void indicated disorder of solvent molecules (ca. $1.3CH_2Cl_2$) in the unit cell, and were squeezed with PLATON program package [52]. In the refinement of **3b**, the N–H hydrogen atoms were calculated at ideal positions and were refined with riding models. The final residual electron densities (ca. $2.9CH_2Cl_2$) in a void were also squeezed [52]. In the refinement of **3c**, the N–H hydrogen atoms were calculated at ideal positions and were refined with riding models.

Acknowledgement

This work was supported by a Grant-in-Aid for Scientific Research (no. 18H03914) and on Priority Area 2802 (no. 17H05374) from the Ministry of Education, Culture, Sports, Science and Technology, Japan. The authors thank Prof. Kohtaro Osakada of Tokyo Institute of Technology for help in MS spectral measurements.

Appendix A. Supplementary data

Supplementary data to this article can be found online at https://doi.org/10.1016/j.jorganchem.2018.10.005.

References

[1] P. Braunstein, L.A. Oro, P.R. Raithby (Eds.), Metal Clusters in Chemistry, vol. 1, Wiley-VCH, Weinheim, 1999.
[2] R.D. Adams, F.A. Cotton (Eds.), Catalysis by Di- and Polynuclear Metal Cluster Complexes, Wiley-VCH, Weinheim, 1998.
[3] R.H. Crabtree, D.M.P. Mingos (Eds.), Comprehensive Organometallic Chemistry III, vol. 12, Elsevier, Oxford, U. K., 2007.
[4] M. Shibasaki, Y. Yamamoto (Eds.), Multimetallic Catalysts in Organic Synthesis, Wiley-VCH, Weinheim, 2004.
[5] S. Sculfort, P. Braunstein, Chem. Soc. Rev. 40 (2011) 2741.
[6] E.J. Fernández, A. Laguna, J.N. López-de-Luzuriaga, Dalton Trans. (2007) 1969.
[7] S.C. Lee, R.H. Holm, Chem. Rev. 104 (2004) 1135.
[8] Y. Takemura, H. Takenaka, T. Nakajima, T. Tanase, Angew. Chem. Int. Ed. 48 (2009) 2157.
[9] Y. Takemura, T. Nakajima, T. Tanase, Eur. J. Inorg. Chem. (2009) 4820.
[10] Y. Takemura, T. Nakajima, T. Tanase, Dalton Trans. (2009) 10231.
[11] Y. Takemura, T. Nishida, B. Kure, T. Nakajima, M. Iida, T. Tanase, Chem. Eur. J. 17 (2011) 10528.
[12] A. Yoshii, H. Takenaka, H. Nagata, S. Noda, K. Nakamae, B. Kure, T. Nakajima, T. Tanase, Organometallics 31 (2012) 133.
[13] T. Tanase, S. Hatada, A. Mochizuki, K. Nakamae, B. Kure, T. Nakajima, Dalton Trans. 42 (2013) 15941.
[14] T. Tanase, R. Otaki, T. Nishida, H. Takenaka, Y. Takemura, B. Kure, T. Nakajima, Y. Kitagawa, T. Tsubomura, Chem. Eur. J. 20 (2014) 1577.
[15] K. Nakamae, B. Kure, T. Nakajima, Y. Ura, T. Tanase, Chem. Asian J. 9 (2014) 3106.
[16] T. Tanase, A. Yoshii, R. Otaki, K. Nakamae, Y. Mikita, B. Kure, T. Nakajima, J. Organomet. Chem. 797 (2015) 37.
[17] K. Nakamae, Y. Takemura, B. Kure, T. Nakajima, Y. Kitagawa, T. Tanase, Angew. Chem. Int. Ed. 54 (2015) 1016.
[18] T. Tanase, S. Hatada, S. Noda, H. Takenaka, K. Nakamae, B. Kure, T. Nakajima, Inorg. Chem. 54 (2015) 8298.
[19] T. Tanase, K. Morita, R. Otaki, K. Yamamoto, Y. Kaneko, K. Nakamae, B. Kure, T. Nakajima, Chem. Eur. J. 23 (2017) 524.
[20] T. Nakajima, Y. Kamiryo, K. Hachiken, K. Nakamae, Y. Ura, T. Tanase, Inorg. Chem. 57 (2018) 11005.
[21] T. Nakajima, S. Kurai, S. Noda, M. Zouda, B. Kure, T. Tanase, Organometallics 31 (2012) 4283.
[22] T. Nakajima, M. Sakamoto, S. Kurai, B. Kure, T. Tanase, Chem. Commun. 49 (2013) 5239.
[23] T. Nakajima, S. Noda, M. Sakamoto, A. Matsui, K. Nakamae, B. Kure, Y. Ura, T. Tanase, Dalton Trans. 45 (2016) 4747.
[24] G. van Koten, D. Milstein (Eds.), Organometallic Pincer Chemistry, Springer, Verlag Berlin Heidelberg, 2013.
[25] D. Morales-Morales (Ed.), Pincer Compounds – Chemistry and Applications, Elsevier, Amsterdam, 2018.
[26] M. Asay, D. Morales-Morales, Dalton Trans. 44 (2015) 17432.
[27] J.M. Serrano-Becerra, H. Valdès, D. Canseco-Gonzáles, V. Gómez-Benítez, S. Hernández-Ortega, D. Morales-Morales, Tetrahedron Lett. 59 (2018) 3377.
[28] H. Valdès, M.A. García-Eleno, D. Canseco-Gonzáles, D. Morales-Morales, ChemCatChem 10 (2018) 3136.
[29] R.C. Bauer, Y. Gloaguen, M. Lutz, J.N.H. Reek, B. de Bruin, J.I. van der Vlugt, Dalton Trans. 40 (2011) 8822, and references cited therein.
[30] M. Mazzeo, M. Strianese, O. Kühl, J.C. Peters, Dalton Trans. 40 (2011) 9026.
[31] A.M. Poitras, S.E. Knight, M.W. Bezpalko, B.M. Foxman, C.M. Thomas, Angew. Chem. Int. Ed. 57 (2018) 1497.
[32] H. Valdès, L. Gonzáles-Sebastián, D. Morales-Morales, J. Organomet. Chem. 845 (2017) 229.
[33] M.M. Greenwood (Ed.), Spectroscopic Properties of Inorganic and Organometallic Compounds, vol. 6, RSC Publishing, UK, 1973.
[34] H.V. Huynh, The Organometallic Chemistry of N-heterocyclic Carbenes, Wiley, West Sussex, UK, 2017.
[35] R.A. Michelin, R. Bertani, M. Mozzon, L. Zanotto, F. Benetollo, G. Bombieri, Organometallics 9 (1990) 1449.
[36] S.-W. Lai, M.C.-W. Chan, K.-K. Cheung, C.-M. Che, Organometallics 18 (1999) 3327.
[37] J. Vicente, A. Arcas, J.M. Fernández-Hernández, Organometallics 26 (2007) 6155.
[38] D. Riedel, T. Wurm, K. Graf, M. Rudolph, F. Rominger, A.S.K. Hashmi, Adv. Synth. Catal. 357 (2015) 1515.
[39] A.S.K. Hashmi, C. Lothschütz, C. Böhling, F. Rominger, Organometallics 30 (2011) 2411.
[40] T.B. Anisimova, M.F.C.G. da Silva, V.Y. Kukushkin, A.J.L. Pombeiro, K.V. Luzyanin, Dalton Trans. 43 (2014) 15861.
[41] V.N. Mikhaylov, V.N. Sorokoumov, K.A. Korvinson, A.S. Novikov, I.A. Balova, Organometallics 35 (2016) 1684.
[42] S. Kundu, W.W. Brennessel, W.D. Jones, Inorg. Chim. Acta. 379 (2011) 109.
[43] D.-A. Roşca, J. Fernandez-Cestau, A.S. Romanov, M. Mochmann, J. Organomet. Chem. 792 (2015) 117.
[44] W. Taniwaki, M. Okazaki, Chem. Lett. 42 (2013) 807.
[45] H.C. Clark, L.E. Manzer, J. Organomet. Chem. 59 (1973) 411.
[46] J.W. Kang, K. Moseley, P.M. Maitlis, J. Am. Chem. Soc. 91 (1969) 5970.
[47] Crystal Clear, Version 1.3.5, Operating Software for the CCD Detector System, Rigaku and Molecular Structure Corp., Tokyo, Japan and The Woodlands, Texas, 2003.
[48] R. Jacobson, REQAB, Molecular Structure Corporation, the Woodlands, Texas, USA, 1998.
[49] G.M. Sheldrick, SHELXS-97 and SHELXL-97: Program for the Solution and the Refinement of Crystal Structures, University of Göttingen, Göttingen, Germany, 1996.
[50] A. Altomare, M. Burla, M. Camalli, G. Cascarano, C. Giacovazzo, A. Guagliardi, A. Moliterni, G. Polidori, R. Spagna, J. Appl. Crystallogr. 32 (1999) 115.
[51] Crystal Structure 4.0, Crystal Structure Analysis Package, Rigaku Corporation, Tokyo 196-8666, Japan, 2000-2010.
[52] A.L. Spek, Acta Crystallogr. D65 (2009) 148.